

A tethering complex drives the terminal stage of SNARE-dependent membrane fusion

Massimo D'Agostino¹, Herre Jelger Risselada^{2,3}, Anna Lürick⁴, Christian Ungermann⁴ & Andreas Mayer¹

Membrane fusion in eukaryotic cells mediates the biogenesis of organelles, vesicular traffic between them, and exo- and endocytosis of important signalling molecules, such as hormones and neurotransmitters. Distinct tasks in intracellular membrane fusion have been assigned to conserved protein systems. Tethering proteins mediate the initial recognition and attachment of membranes, whereas SNARE (soluble N-ethylmaleimide-sensitive factor attachment protein receptor) protein complexes are considered as the core fusion engine. SNARE complexes provide mechanical energy to distort membranes and drive them through a hemifusion intermediate towards the formation of a fusion pore^{1–3}. This last step is highly energy-demanding^{4,5}. Here we combine the *in vivo* and *in vitro* fusion of yeast vacuoles with molecular simulations to show that tethering proteins are critical for overcoming the final energy barrier to fusion pore formation. SNAREs alone drive vacuoles only into the hemifused state. Tethering proteins greatly increase the volume of SNARE complexes and deform the site of hemifusion, which lowers the energy barrier for pore opening and provides the driving force. Thereby, tethering proteins assume a crucial mechanical role in the terminal stage of membrane fusion that is likely to be conserved at multiple steps of vesicular traffic. We therefore propose that SNAREs and tethering proteins should be considered as a single, non-dissociable device that drives fusion. The core fusion machinery may then be larger and more complex than previously thought.

SNAREs dock membranes by stepwise assembly into four-helix bundles. They exert mechanical force through their transmembrane domains (TMDs)^{1,2}. This induces the fusion of the outer leaflets (hemifusion), followed by inner leaflet fusion and pore formation. Pore formation can be preceded by full zipping of the four-helix bundle⁶. Fusion is often studied with synaptic SNAREs, which use unique cofactors to fuse highly curved neurotransmitter vesicles with exquisite speed and temporal control⁷. The membranes in most other fusion reactions fuse more slowly, are much less curved, and their SNARE density is lower. Fusion driven solely by SNAREs becomes much less effective with increasing vesicle diameter and decreasing SNARE density^{8,9}. In these conditions, multi-subunit tethering complexes become important. These facilitate membrane contact, associate with the SNARE-binding Sec1/Munc18-like (SM) proteins^{10–12} and promote *trans*-SNARE pairing. We investigated whether tethering complexes enhance the fusogenic potential of SNARE complexes by increasing the force that SNAREs transmit to the bilayers, or by lowering the energy barrier for fusion pore formation.

The homotypic fusion and protein sorting complex (HOPS) is the tethering complex for vacuole and lysosome fusion. Vacuoles from cells that do not express the Rab-GTPase Ypt7 lack HOPS¹³ (Extended Data Fig. 1a). This prevents fusion and pairing between the vacuolar SNAREs Vam3, Vti1, Vam7 and Nyv1¹⁴. Incubating these membranes with soluble, recombinant vacuolar Q_c-SNARE Vam7

(rVam7) enables the stimulation of *trans*-SNARE pairing. Under these conditions, the reaction is independent of endogenous Vam7, which must otherwise be liberated by Sec18 (also known as soluble N-ethylmaleimide-sensitive factor, NSF)-dependent disruption of *cis*-SNARE complexes¹⁵. Fusion can hence proceed without ATP, avoiding interference by the ATP-driven chaperone Sec18, which disassembles SNARE complexes unless HOPS protects them¹⁴. To assay *trans*-SNARE pairing, we separately prepared vacuoles from *ypt7Δ* or wild-type strains expressing haemagglutinin (HA)-tagged Nyv1 (Nyv1-HA) or Myc-tagged Vam3 (Vam3-Myc). We mixed them in fusion reactions with rVam7 and measured *trans*-SNARE pairing through co-immunoadsorption of Vam3-Myc with Nyv1-HA. Adding rVam7 to *ypt7Δ* vacuoles induced similar *trans*-SNARE pairing as in wild-type vacuoles (Fig. 1a, b). We measured content mixing by transfer of a 45 kDa enzyme between the fusion partners (Extended Data Fig. 2), and lipid mixing by fluorescence dequenching through dilution of rhodamine-labelled phosphatidylethanolamine^{3,16}. The *trans*-SNARE complexes on *ypt7Δ* vacuoles failed to induce content mixing (Fig. 1c), whereas lipid mixing was similar to wild-type vacuoles (Fig. 1d, e). Thus, HOPS-free *ypt7Δ* vacuoles reached a hemifused state but failed to form a fusion pore, or to open it wide enough to let the reporter pass. Lipid mixing was sensitive to antibodies targeting the Q_a-SNARE Vam3 or the R-SNARE Nyv1, confirming that the reaction was SNARE-dependent. The *ypt7Δ trans*-SNARE complexes are probably fully zippered, because this is a prerequisite for lipid mixing¹⁷.

To test the effect of HOPS on pore opening, we accumulated *ypt7Δ* vacuoles for 60 min in the hemifused state, added purified HOPS or HOPS subcomplexes (Extended Data Fig. 1b), and assayed content mixing after 15 min of further incubation. HOPS is a hexameric complex with a globular SNARE-binding domain that contains the SNARE-binding SM protein Vps33 and its interactor Vps16¹⁸ (Fig. 1f). Vps33 alone (79 kDa) did not stimulate fusion (Fig. 1g), whereas the bigger Vps33–Vps16 subcomplex (159 kDa) rescued fusion to 80% of an untreated wild-type control that had been incubated under standard fusion conditions with ATP. A Vps11–Vps39 subcomplex (240 kDa), representing the opposite end of HOPS without a SNARE interaction site, had no effect (Fig. 1g). As the biggest structure, HOPS (663 kDa) rescued *ypt7Δ* fusion to wild-type levels. The endosomal class C core vacuole/endosome tethering (CORVET) complex, which is a similar size to HOPS and also contains Vps33¹¹, stimulated fusion as well as HOPS (Extended Data Fig. 3). The specificity of these complexes is hence restricted to their Rab-GTPase-dependent function in membrane tethering. HOPS did not enhance *trans*-SNARE pairing beyond the level attained by the preincubation with rVam7 (Fig. 1a, b). Nevertheless, rescue was SNARE-dependent because HOPS did not induce fusion in the absence of Vam7, nor upon preincubation of the vacuoles with antibodies to Vam3 (Fig. 1g and Extended Data Fig. 4). These results suggest an additional role of HOPS in fusion pore opening that is independent of its known role in facilitating SNARE pairing^{12,19}.

¹Département de Biochimie, Université de Lausanne, Chemin des Boveresses 155, CH-1066 Epalinges, Switzerland. ²Georg-August University, Department of Theoretical Physics, Göttingen, Friedrich-Hund-Platz 1, D-37077 Göttingen, Germany. ³Leibniz Institute of Surface Modification, Chemical Department, Permoserstrasse 15, D-04318, Leipzig, Germany. ⁴University of Osnabrück, Department of Biology/Chemistry, Barbarastrasse 13, D-49076 Osnabrück, Germany.

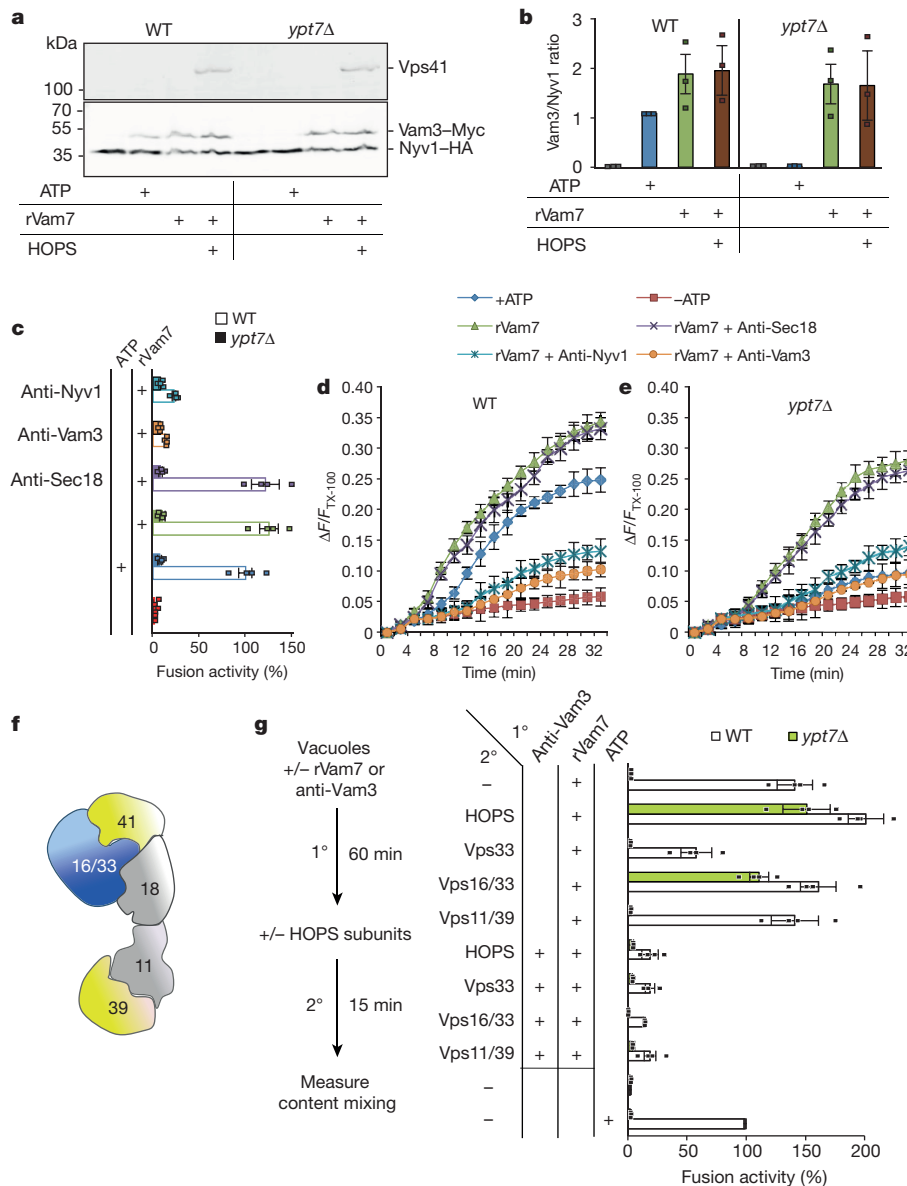


Figure 1 | Effect of soluble Vam7 on lipid and content mixing.

a, b, Trans-SNARE pairing. Vacuoles were isolated from wild-type (BJ3505, WT) or isogenic *ypt7Δ* cells carrying Vam3-Myc or Nyv1-HA. The two vacuole populations were mixed and incubated in fusion reactions with ATP, Vam7 and HOPS as indicated. Proteins were solubilized, pulled down with anti-haemagglutinin antibody and analysed by SDS-PAGE and western blotting (**a**). *Trans*-SNARE pairing is assessed by Vam3-Myc co-adsorbed to Nyv1-HA. Bands were quantified (**b**). **c–e, Hemifusion in *ypt7Δ* vacuoles.** Vacuoles from wild-type and *ypt7Δ* cells were incubated in ATP-free fusion reactions with 600 nM rVam7 and 10 mg ml⁻¹ BSA. Antibodies (200 nM) had been added where indicated. **c, Content mixing determined after 60 min, using the activation of pro-alkaline phosphatase by a maturase from the fusion partners.**

To test whether pore opening might be driven by increased SNARE complex volume, we accumulated hemifused *ypt7Δ* vacuoles and added calmodulin binding peptide (CBP)-tagged Vps33, which does not stimulate pore opening. When we tripled the effective molecular mass of Vps33 by adding a monoclonal antibody (150 kDa) to its CBP tag, content mixing increased fivefold and reached more than 50% of the wild-type signal (Fig. 2a). Antibodies did not stimulate fusion when Vps33 had been omitted, nor when Vps33 was used with a non-cognate haemagglutinin-antibody. CBP-Vps33 alone decreased the content mixing of wild-type vacuoles by 60%, and this inhibition could be partially overcome by adding CBP antibodies. This can be understood

d, e, Lipid mixing was followed by dequenching of the fluorescence of rhodamine-labelled phosphatidylethanolamine, which had been integrated at self-quenching concentrations into one of the fusion partners. Fluorescence dequenching (ΔF) was measured relative to the maximal dequenching obtained after solubilising the system in Triton X-100 (F_{TX-100}). **f, Structure of HOPS (adapted from ref. 18).** **g, Effect of HOPS subcomplexes on content mixing.** Vacuoles were first incubated (1°) in fusion reactions as in **c** for 60 min, with anti-Vam3 antibody where indicated. The samples then received 400 nM purified CBP-tagged HOPS subcomplexes or Vps33 and were incubated for a further 15 min (2°) before content mixing was assayed. Data in **b–e** and **g** are mean \pm s.d. from 3 biologically independent experiments.

if CBP-Vps33 outcompetes endogenous HOPS for SNARE binding but by itself does not add sufficient mass to stimulate fusion.

Next, we replaced HOPS with artificial SNARE-binding proteins, using only polyclonal antibodies to SNAREs (Fig. 2b). When added at the beginning of a reaction, SNARE antibodies interfere with *trans*-SNARE pairing and block fusion. To circumvent this block, we first accumulated *ypt7Δ* vacuoles in the hemifused state, with *trans*-SNARE complexes already formed. Under these conditions, anti-Nyv1 or anti-Vam3 antibodies became strong stimulators. They rescued content mixing to 50% when added individually and to 100% when added simultaneously. Wild-type vacuoles, which contain sufficient amounts

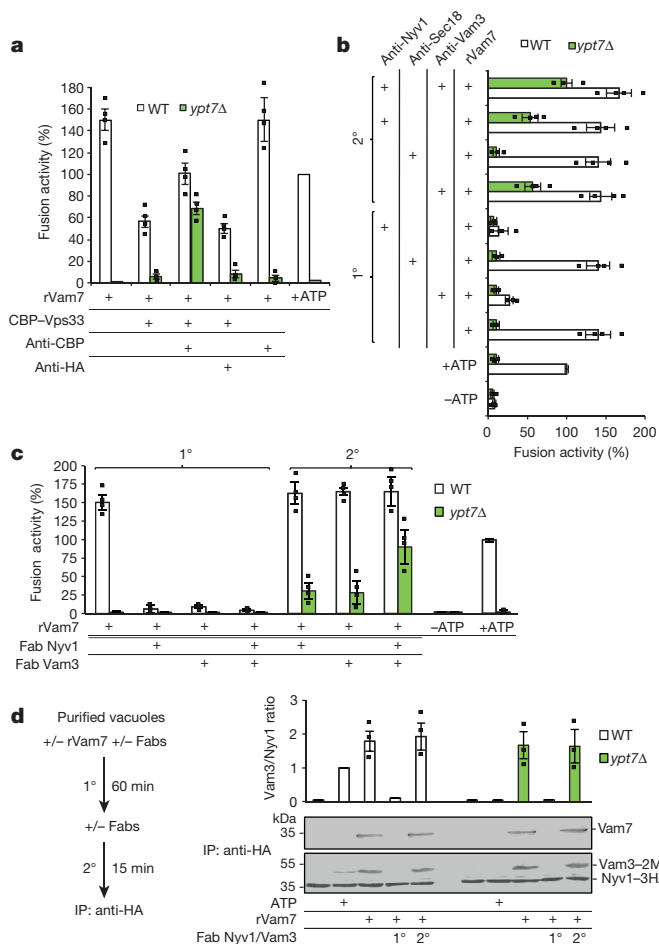


Figure 2 | Fusion pore opening driven by ligands increasing SNARE complex size *in vitro*. **a**, Vps33 as a ligand. Fusion reactions with wild-type and *ypt7Δ* vacuoles were started as in Fig. 1g. After the first 60-min incubation period, samples received recombinant CBP-Vps33 (400 nM), antibodies to CBP or haemagglutinin (200 nM), or buffer only. After a further 15 min, content mixing was assayed. **b**, Antibodies as ligands. Two-stage fusion reactions were performed as in **a**, but only with rVam7. Antibodies (200 nM) against Vam3, Nyv1 or Sec18 were added either during the first 60 min incubation or during the second incubation of 15 min. **c**, Fabs as ligands. Experiment as in **b**, but with Fabs instead of antibodies. **d**, *Trans*-SNARE pairing was assayed using tagged strains as in Fig. 1a. Reactions with staged addition of rVam7 and Fabs were run as in **c**. IP, immunoprecipitation. Data are mean \pm s.d. from 3 biologically independent experiments.

of endogenous HOPS, were hardly stimulated by the antibodies. Thus, artificial SNARE ligands substitute for HOPS in fusion pore opening *in vitro*.

Since bivalent antibodies to SNAREs might promote fusion by clustering SNARE complexes around a fusion site, we generated monovalent antigen-binding fragments (Fabs) from them (Extended Data Fig. 1c). These inhibited fusion and *trans*-SNARE pairing when added before docking (Fig. 2c, d), but they potently stimulated content mixing of hemifused vacuoles without affecting *trans*-SNARE pairing. Individual use of Fabs to either Vam3 or Nyv1 stimulated fusion weakly, probably because Fabs are smaller (56 kDa) than IgGs (150 kDa), and their dimensions permit the placement of no more than two Fabs along a SNARE domain. Two Fabs to a single SNARE may therefore not add sufficient volume to SNARE complexes to drive pore opening. Crowding agents²⁰, such as Ficoll 400, had no influence, suggesting that bulky SNARE complex ligands do not stimulate fusion by molecular crowding (Extended Data Figs 5, 3). Thus, HOPS may promote fusion pore formation *in vitro* by increasing the volume of SNARE complexes.

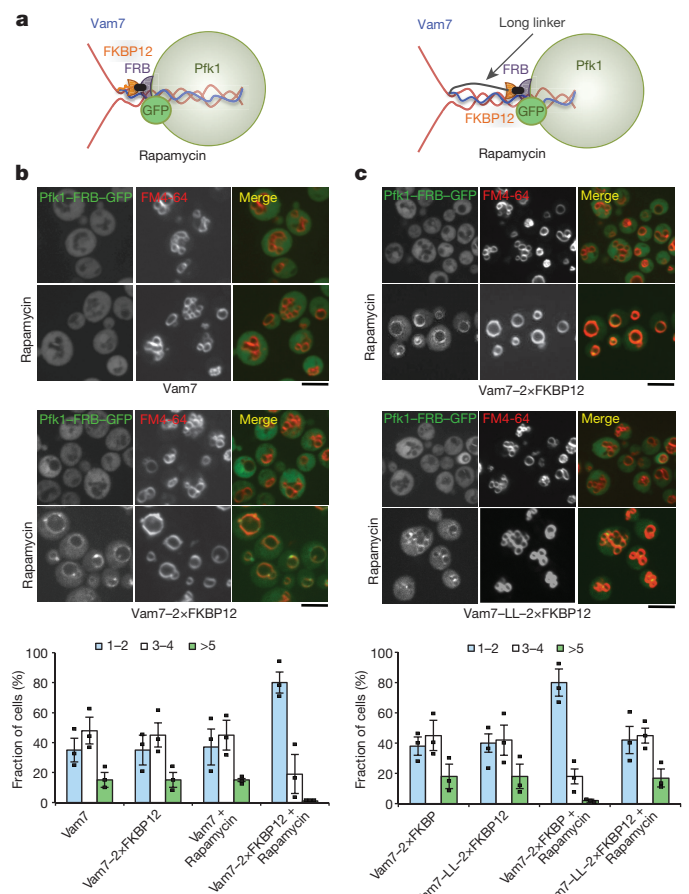


Figure 3 | Effect of SNARE complex enlargement on vacuole fusion *in vivo*. **a**, Schematic view of rapamycin-induced FKBP12/FRB-tagged Pfk1 recruitment to the SNARE complex without and with a long linker (LL; 35 amino acids) between Vam7 and FKBP12. **b, c**, *In vivo* vacuole morphology. Logarithmically growing cells, carrying Pfk1-FRB-GFP and Vam7 or Vam7-2 \times FKBP12 (b, top or bottom images respectively), or Pfk1-FRB-GFP and Vam7-2 \times FKBP12 or Vam7-LL-2 \times FKBP12 (c, top or bottom pictures respectively), were stained with the vacuole tracer FM4-64. Cells were incubated with 10 μ M rapamycin for 10 min where indicated and analysed by spinning disc microscopy. The cells were grouped into three categories according to the number of vacuoles visible per cell. 100 cells were analysed per sample. Scale bars, 5 μ m. Data are mean \pm s.d. from 3 biologically independent experiments.

We engineered an *in vivo* system for recruiting large ligands to SNAREs using FKBP12 and FRB, two domains that undergo rapamycin-induced dimerization²¹. FKBP12 (12 kDa) was attached to the C terminus of Vam7, which is close to the TMDs of the SNARE complex. Green fluorescent protein (GFP)-tagged FRB (FRB-GFP) (38 kDa) was attached to Pfk1, a subunit of the octameric, soluble phosphofructokinase (850 kDa), which is unrelated to fusion (Fig. 3a and Extended Data Fig. 1d, e). Rapamycin-insensitive *tor1-1* cells served as a background strain to avoid side effects of rapamycin treatment through TOR signalling²². Under normal growth conditions, *tor1-1* cells have multiple vacuoles. Rapamycin recruited Pfk1-FRB-GFP to vacuoles within less than 10 min (Fig. 3b, c). These vacuoles fused, significantly reducing their number per cell. Recruitment, but not fusion, was observed when FKBP12 was separated from Vam7 by a 35-amino-acid linker (Fig. 3c). Vam7 lacking FKBP12 induced neither recruitment nor fusion (Fig. 3b), and a FRB-GFP chimera that lacked phosphofructokinase did not induce fusion (Extended Data Fig. 6).

HOPS recruitment controls the re-fusion of vacuoles following hypertonic shock^{23,24}. Hypertonic shock fragments yeast vacuoles in less than 5 min, and Vps41 becomes phosphorylated through the

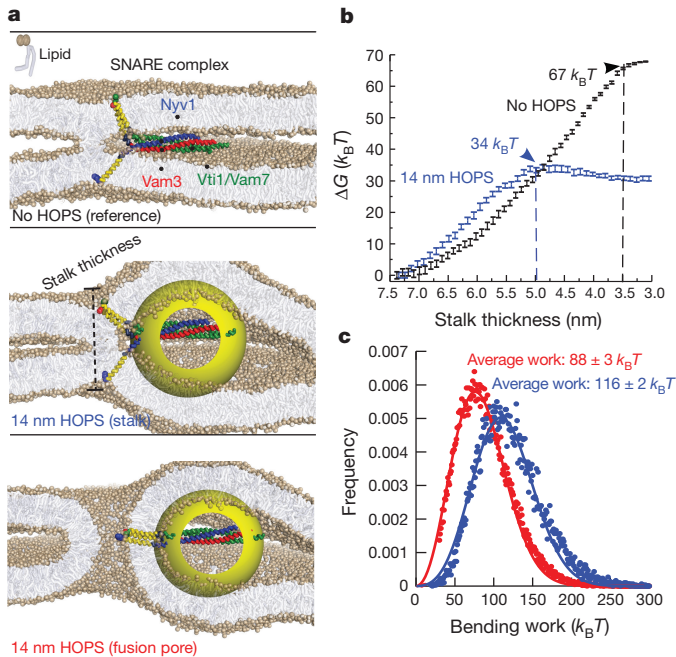


Figure 4 | Molecular dynamics simulations of the influence of steric constraints at the (hemi)fusion site. **a**, Simulation setup: two hemifused membranes in the presence of the SNARE complex that is either free or bound to a sphere equivalent to the size of the SNARE-binding domain of HOPS (14 nm). Dimensions and the relative positioning are inspired by electron microscopy and crystal structures^{9,11,18}. To enhance clarity, only one SNARE complex is illustrated. **b**, The free energy of fusion pore formation is derived by measuring the work (free energy) required to thin the stalk until fusion pore nucleation occurs³² (see Extended Data Fig. 8). Arrowheads and dotted lines indicate the point of pore nucleation. Error bars are calculated via Bayesian resampling using the weighted histogram analysis method (WHAM) on 50 overlapping histograms. Each parental WHAM histogram consists of more than 30,000 data points (autocorrelation up to approximately 1,500 data points). **c**, Work distribution reflecting the equilibrium work that HOPS must perform to bend the membrane in the presence of a stalk (blue, average work: $116 \pm 2 k_B T$ (s.e.m.)) or of a fusion pore (red, average work: $88 \pm 3 k_B T$ (s.e.m.)), respectively. A reduction of approximately $30 k_B T$ indicates that fusion pore formation is associated with release of local membrane stress.

kinase Yck3, which impairs Vps41 concentration at membrane-membrane interfaces and vacuole refusion. While re-fusion requires less than 60 min in wild-type cells, rapamycin-induced recruitment of Pfk1-FRB-GFP to SNAREs provoked premature fusion of these vacuolar fragments, circumventing the physiological inactivation of HOPS (Extended Data Fig. 7). Fusion was not observed in cells lacking FKBP12 on Vam7, nor when rapamycin was omitted.

We explored the influence of bulky SNARE ligands by coarse-grained molecular dynamics (Fig. 4a). HOPS features a SNARE-binding domain approximately 12–14 nm in diameter, and this probably encapsulates the SNARE complex^{11,18} (Fig. 1f). Binding a sphere the size of this head region to SNAREs markedly affects the geometry of the hemifusion stalk (Fig. 4a). The stalk restrains the apposed membranes from separating, and enforces strong local curvature. We rationalized the acceleration of fusion from the apparent work (free energy) required to thin the hemifusion stalk (Fig. 4a, b and Supplementary Information). Progression from hemifusion to pore opening decreases the mutual distance of the SNARE C termini until they associate (Fig. 4a). The presence of a HOPS sphere (14 nm) halves the energetic cost of fusion pore opening (from $67 k_B T$ to $34 k_B T$) in a tensionless membrane system with three SNARE complexes (Fig. 4b and Extended Data Fig. 8). Pore nucleation now requires far less thinning of the stalk. We attribute the enhanced (non-leaky) fusion pore formation to a partial, relative relaxation of the HOPS-induced curvature stress (approximately $30 k_B T$)

(Fig. 4c and Extended Data Fig. 9), and a geometrical advantage because of the pre-existing curvature (Extended Data Fig. 8). Smaller contributions can be made by an initial gain in the SNARE pulling force (Extended Data Fig. 10). HOPS thus stimulates pore opening by steric effects on the site of hemifusion. These aspects are elaborated in Supplementary Discussion.

We can understand numerous unexplained findings from this perspective: (1) SNARE-associated tethering complexes (Munc13 and its associated SM protein Munc18) are essential for fusion of synaptic vesicles. While this can reflect their role in SNARE complex assembly, Munc13 and Munc18 might also drive fusion itself²⁵. Accordingly, mutations that reduce the affinity of Munc18 for SNAREs change fusion pore dynamics²⁶. (2) Mutating the yeast Munc18 homologue Sec1, which associates with the tethering complex exocyst²⁷, reduces exocytosis without reducing SNARE complex abundance^{28,29}. (3) On vacuoles, mutations that compromise Vps33 binding to vacuolar SNAREs impair content mixing more than lipid mixing and *trans*-SNARE pairing¹⁶. (4) HOPS also enhances liposome fusion more than *trans*-SNARE pairing³⁰. (5) Binding to Sec17 (also known as α -SNAP) and Sec18 renders *trans*-SNARE complexes more fusogenic^{17,31}.

Our simulations and experimental observations suggest that bulky SNARE-ligands can drive fusion irrespective of all specific molecular properties, except for their size. Since SM proteins and tethering complexes are indispensable for fusion in multiple trafficking pathways¹¹, we propose that the driving force that they can contribute to fusion is a critical and conserved feature of their function. In physiological membranes, SNAREs and their tethering-SM protein complexes thus act as an integrated molecular machine, in which tethering and SM proteins first facilitate SNARE pairing¹¹ and then drive the very last step of fusion.

Online Content Methods, along with any additional Extended Data display items and Source Data, are available in the online version of the paper; references unique to these sections appear only in the online paper.

Received 28 February; accepted 3 October 2017.

Published online 1 November 2017.

- Gao, Y. *et al.* Single reconstituted neuronal SNARE complexes zipper in three distinct stages. *Science* **337**, 1340–1343 (2012).
- Zhang, X. *et al.* Stability, folding dynamics, and long-range conformational transition of the synaptic t-SNARE complex. *Proc. Natl Acad. Sci. USA* **113**, E8031–E8040 (2016).
- Reese, C., Heise, F. & Mayer, A. *Trans*-SNARE pairing can precede a hemifusion intermediate in intracellular membrane fusion. *Nature* **436**, 410–414 (2005).
- Chernomordik, L. V. & Kozlov, M. M. Protein-lipid interplay in fusion and fission of biological membranes. *Annu. Rev. Biochem.* **72**, 175–207 (2003).
- Cohen, F. S. & Melikyan, G. B. The energetics of membrane fusion from binding, through hemifusion, pore formation, and pore enlargement. *J. Membr. Biol.* **199**, 1–14 (2004).
- Shin, J., Lou, X., Kweon, D.-H. & Shin, Y.-K. Multiple conformations of a single SNAREpin between two nanodisc membranes reveal diverse pre-fusion states. *Biochem. J.* **459**, 95–102 (2014).
- Rizo, J. & Südhof, T. C. The membrane fusion enigma: SNAREs, Sec1/Munc18 proteins, and their accomplices—guilty as charged? *Annu. Rev. Cell Dev. Biol.* **28**, 279–308 (2012).
- Hernandez, J. M., Kreuzberger, A. J. B., Kiessling, V., Tamm, L. K. & Jahn, R. Variable cooperativity in SNARE-mediated membrane fusion. *Proc. Natl Acad. Sci. USA* **111**, 12037–12042 (2014).
- Baker, R. W. *et al.* A direct role for the Sec1/Munc18-family protein Vps33 as a template for SNARE assembly. *Science* **349**, 1111–1114 (2015).
- Orr, A., Wickner, W., Rusin, S. F., Kettenbach, A. N. & Zick, M. Yeast vacuolar HOPS, regulated by its kinase, exploits affinities for acidic lipids and Rab:GTP for membrane binding and to catalyze tethering and fusion. *Mol. Biol. Cell* **26**, 305–315 (2015).
- Kuhlee, A., Raunser, S. & Ungermann, C. Functional homologies in vesicle tethering. *FEBS Lett.* **589**, 2487–2497 (2015).
- Zick, M. & Wickner, W. The tethering complex HOPS catalyzes assembly of the soluble SNARE Vam7 into fusogenic *trans*-SNARE complexes. *Mol. Biol. Cell* **24**, 3746–3753 (2013).
- Price, A., Seals, D., Wickner, W. & Ungermann, C. The docking stage of yeast vacuole fusion requires the transfer of proteins from a *cis*-SNARE complex to a Rab/Ypt protein. *J. Cell Biol.* **148**, 1231–1238 (2000).
- Xu, H., Jun, Y., Thompson, J., Yates, J. & Wickner, W. HOPS prevents the disassembly of *trans*-SNARE complexes by Sec17p/Sec18p during membrane fusion. *EMBO J.* **29**, 1948–1960 (2010).

15. Thorngren, N., Collins, K. M., Fratti, R. A., Wickner, W. & Merz, A. J. A soluble SNARE drives rapid docking, bypassing ATP and Sec17/18p for vacuole fusion. *EMBO J.* **23**, 2765–2776 (2004).
16. Pieren, M., Schmidt, A. & Mayer, A. The SM protein Vps33 and the t-SNARE H_{abc} domain promote fusion pore opening. *Nat. Struct. Mol. Biol.* **17**, 710–717 (2010).
17. Schwartz, M. L. & Merz, A. J. Capture and release of partially zipped *trans*-SNARE complexes on intact organelles. *J. Cell Biol.* **185**, 535–549 (2009).
18. Bröcker, C. *et al.* Molecular architecture of the multisubunit homotypic fusion and vacuole protein sorting (HOPS) tethering complex. *Proc. Natl Acad. Sci. USA* **109**, 1991–1996 (2012).
19. Orr, A., Song, H., Rusin, S. F., Kettenbach, A. N. & Wickner, W. HOPS catalyzes the interdependent assembly of each vacuolar SNARE into a SNARE complex. *Mol. Biol. Cell* **28**, 975–983 (2017).
20. Yu, H. *et al.* Reconstituting intracellular vesicle fusion reactions: the essential role of macromolecular crowding. *J. Am. Chem. Soc.* **137**, 12873–12883 (2015).
21. Haruki, H., Nishikawa, J. & Laemmli, U. K. The anchor-away technique: rapid, conditional establishment of yeast mutant phenotypes. *Mol. Cell* **31**, 925–932 (2008).
22. Michailat, L., Baars, T. L. & Mayer, A. Cell-free reconstitution of vacuole membrane fragmentation reveals regulation of vacuole size and number by TORC1. *Mol. Biol. Cell* **23**, 881–895 (2012).
23. Cabrera, M. *et al.* Vps41 phosphorylation and the Rab Ypt7 control the targeting of the HOPS complex to endosome–vacuole fusion sites. *Mol. Biol. Cell* **20**, 1937–1948 (2009).
24. LaGrassa, T. J. & Ungermann, C. The vacuolar kinase Yck3 maintains organelle fragmentation by regulating the HOPS tethering complex. *J. Cell Biol.* **168**, 401–414 (2005).
25. Carr, C. M. & Rizo, J. At the junction of SNARE and SM protein function. *Curr. Opin. Cell Biol.* **22**, 488–495 (2010).
26. Fisher, R. J., Pevsner, J. & Burgoyne, R. D. Control of fusion pore dynamics during exocytosis by Munc18. *Science* **291**, 875–878 (2001).
27. Morgera, F. *et al.* Regulation of exocytosis by the exocyst subunit Sec6 and the SM protein Sec1. *Mol. Biol. Cell* **23**, 337–346 (2012).
28. Hashizume, K., Cheng, Y.-S., Hutton, J. L., Chiu, C.-H. & Carr, C. M. Yeast Sec1p functions before and after vesicle docking. *Mol. Biol. Cell* **20**, 4673–4685 (2009).
29. Grote, E., Carr, C. M. & Novick, P. J. Ordering the final events in yeast exocytosis. *J. Cell Biol.* **151**, 439–452 (2000).
30. Zick, M. & Wickner, W. T. A distinct tethering step is vital for vacuole membrane fusion. *Elife* **3**, e03251 (2014).
31. Zick, M., Orr, A., Schwartz, M. L., Merz, A. J. & Wickner, W. T. Sec17 can trigger fusion of *trans*-SNARE paired membranes without Sec18. *Proc. Natl Acad. Sci. USA* **112**, E2290–E2297 (2015).
32. Risselada, H. J., Bubnis, G. & Grubmüller, H. Expansion of the fusion stalk and its implication for biological membrane fusion. *Proc. Natl Acad. Sci. USA* **111**, 11043–11048 (2014).

Supplementary Information is available in the online version of the paper.

Acknowledgements We thank V. Comte and J. Gao for the purification of proteins and antibodies. This work was supported by grants from the DFG (SFB 944, to C.U.), State of Lower Saxony (life@nano, to H.J.R.) and SNF and ERC to A.M. HLRN is acknowledged for CPU time.

Author Contributions H.J.R. conceived and interpreted simulation experiments and values derived from them. M.D.A. conceived, performed and interpreted all other experiments. A.M. conceived the study and interpreted the results. A.L. and C.U. provided purified CORVET, HOPS and HOPS subcomplexes. All authors jointly wrote the paper.

Author Information Reprints and permissions information is available at www.nature.com/reprints. The authors declare no competing financial interests. Readers are welcome to comment on the online version of the paper. Publisher's note: Springer Nature remains neutral with regard to jurisdictional claims in published maps and institutional affiliations. Correspondence and requests for materials should be addressed to A.M. (andreas.mayer@unil.ch).

METHODS

Strains and cell culture conditions. All strains were grown in either in YPD (yeast extract, peptone, dextrose) containing 2% glucose in the presence or absence of G418, or in SC (synthetic dextrose) dropout media containing 2% glucose to select for auxotrophies. Strains used in this study can be found in Supplementary Table 1. Primers used can be found in Supplementary Table 2. Vam7-LL-2×FKBP12 contains a linker (LL) of 35 amino acids with the sequence SGGGSGGGSGGGSGGGSGGGSGGGSGGGGAAGG.

Genetic manipulations. Yeast transformations were carried out using the lithium acetate method. Gene deletions and tagging were performed as previously established^{33,34}. Genome-tagging of Vam7 with 2×FKBP12 and LL-2×FKBP12 was performed starting from the plasmid pKT209, from which GFP was removed by double digestion with PacI and AscI restriction enzymes and replaced by a 2×FKBP12 coding sequence carrying the same restriction sites. The 2×FKBP12 sequence was obtained by gene synthesis (BIOCAT) and cloned into a pUC57 vector. pRS415-TEFpr-FRB-GFP was obtained starting from a pRS416-53-FRB-GFP vector (provided by C.U.'s group). The FRB-GFP coding frame was amplified by PCR using the primers reported above and cloned into the pRS415-TEFpr vector using HindIII and SacI restriction sites.

Vacuole isolation. BJ3505 and DKY6281 strains carrying tagged SNAREs were grown in YPD at (30°C, 225 r.p.m.) to OD_{600 nm} = 1 and collected (3 min, 5,000g). Collected cells were resuspended in reduction buffer (30 mM Tris-HCl, pH 8.9, 10 mM dithiothreitol (DTT)) and incubated for 5 min at 30°C. After collecting as described above, cells were resuspended in 15 ml digestion buffer (600 mM sorbitol, 50 mM potassium phosphate pH 7.5 in YP medium with 0.2% glucose and 0.1 mg ml⁻¹ lyticase preparation). After 25 min at 30°C, cells were centrifuged (2 min, 3,250g, JA25.50 rotor). The spheroblasts were resuspended in 2 ml 15% Ficoll-400 in PS buffer (10 mM PIPES/KOH pH 6.8, 200 mM sorbitol) and 150 µl (for DKY6281-derived strains) or 250 µl (for BJ3505 derivatives) DEAE dextran (0.4 mg ml⁻¹ in PS buffer). After 2 min of incubation at 30°C, the cells were transferred to SW41 tubes and overlaid with steps of 8%, 4% and 0% Ficoll-400 in PS buffer. Cells were centrifuged for 90 min at 4°C and 153,900g in a SW41 rotor. Lyticase had been recombinantly expressed in *Escherichia coli* RSB805 (provided by R. Schekman) and prepared from a periplasmic supernatant³.

Vacuole fusion and content mixing assay. DKY6281 and BJ3505 vacuoles were adjusted to a protein concentration of 0.5 mg ml⁻¹ and incubated in a volume of 30 µl PS buffer with 125 mM KCl, 0.5 mM MnCl₂. Note that the harvested vacuole suspension contains around 20 mg ml⁻¹ Ficoll-400, creating an environment of moderate molecular crowding³⁵. Vacuoles were preincubated with inhibitors on ice (5 min) before starting the fusion by addition of the ATP-regenerating system (0.25 mg ml⁻¹ creatine kinase, 20 mM creatine phosphate, 500 µM ATP, 500 µM MgCl₂) or of 600 nM rVam7 and 10 mg ml⁻¹ BSA. Samples were incubated for 60 min at 27°C. Two-stage reactions included a second 15-min incubation at 27°C, during which 200 nM antibodies or 400 nM purified HOPS subunits were added. In order to assay fusion, 1 ml of PS buffer was added, vacuoles were centrifuged (2 min, 20,000g, 4°C) and resuspended in 500 µl developing buffer (10 mM MgCl₂, 0.2% Triton X-100, 250 mM Tris-HCl pH 8.9, 1 mM *p*-nitrophenylphosphate). After 5 min at 27°C, the reactions were stopped with 500 µl 1 M glycine pH 11.5 and the OD was measured at 405 nm. Background activity of pro-Pho8 was assessed through a fusion sample kept on ice throughout the incubation period. The value of this sample was subtracted from the others.

Lipid mixing assay. Lipid mixing was assayed as described³. In brief, 30 µg of unlabelled BJ3505 vacuoles and 6 µg of rhodamine-labelled phosphatidylethanolamine DKY6281 vacuoles were mixed in 190 µl of 0.3 mM MnCl₂, 75 mM KCl in PS buffer. Inhibitors were pre-warmed to 27°C before being added to the tubes. Fusion reactions were started by adding 9.5 µl of 20× ATP-regenerating system, yielding 0.125 mg ml⁻¹ creatine kinase, 20 mM creatine phosphate, 0.5 mM ATP, 0.5 mM MgCl₂. 100 µl of this mixture was used to assay lipid mixing in a fluorescent plate reader at 27°C for 32 min. 80 µl were incubated separately for 60 min and then assayed for content mixing by alkaline phosphatase developing buffer as described above.

Immunoprecipitations. Vacuoles from a 1 ml fusion reaction were pelleted (5 min, 6,000g, 4°C), solubilized for 10 min in lysis buffer (0.5% Triton X-100, 0.5 mM MnCl₂, 100 mM CaCl₂, 1 mM phenylmethylsulfonyl fluoride (PMSF)) and centrifuged (10 min at 12,000g and 4°C). The supernatant was supplemented with 30 µg of antibody and 25 µl of protein-G sepharose and shaken for 60 min at 4°C. The beads were washed three times with lysis buffer and suspended in SDS sample buffer.

Gel electrophoresis and western blot. Protein samples were dissolved in reducing sample buffer and heated to 95°C for 5 min. The samples were run on either 10% or 12.5% polyacrylamide gels. The stacking gels were prepared as follows: 6% acrylamide, 0.16% bis-acrylamide, 0.1 M Tris pH 6.8, 0.1% SDS, 0.1% TEMED, 0.05% ammonium persulfate. Running gels were: 10% or 12.5% acrylamide, 0.27%

or 0.34% bis-acrylamide, 0.38 M Tris pH 8.8, 0.1% SDS, 0.06% TEMED, 0.06% APS. The gels (10 cm/8 cm/1.5 mm) were run at constant current (20–30 mA). Proteins were blotted onto nitrocellulose membrane by the semi-dry method for 80 min at 400 mA. After incubation with the primary antibody overnight, signals were detected by secondary antibodies coupled to infrared dyes and detected on a LICOR Odyssey infrared laser scanner. Images were exported as TIFF files and processed in Adobe Illustrator CS3. Band intensity was quantified using densitometry software supplied with the Odyssey Infrared Imager.

FM4-64 staining. Cells were inoculated from a pre-culture in stationary phase and grown overnight to logarithmic phase (OD_{600 nm} between 0.2 and 0.8). After dilution to an OD_{600 nm} of 0.2 in 1 ml culture, FM4-64 (*N*-(3-triethylammoniumpropyl)-4-(6-(4-(diethylamino) phenyl) hexatrienyl) pyridinium dibromide) in DMSO was added to a final concentration of 10 µM. Cells were stained for 1 h, followed by three washing steps in medium without stain (2 min, 3,000g) and a subsequent chase of 1 to 2 h in medium without stain, depending on the endocytotic capacity of the strain. The cells for microscopy were grown at 30°C. The temperature was kept constant during staining and visualization. Care was taken to analyse cells immediately after their removal from the culture tube.

Antibodies and affinity purification. Sources of monoclonal antibodies were: anti-HA (16B12, MMS-101P, Covance); anti-Myc (9E11, sc-47694, Santa Cruz Biotechnology). Polyclonal antibodies against Vam3, Nyy1, Vam7, Vps39, Ypt7 and GFP were raised by injecting purified recombinant hydrophilic parts of these proteins into rabbits. Antibodies were purified from sera. Sera were first heated for 30 min at 56°C to inactivate the complement system, diluted 1:1 in PBS and filtered through 0.2-µm membranes before being passed onto an activated CH-sepharose 4B column (GE Healthcare Life Sciences 17-0430-01), which had been coupled with the recombinant protein of interest, according to the instructions of the manufacturer. The column was washed with ten bed volumes of PBS at 4°C. The antibodies were eluted with 0.2 M glycine-HCl pH 2.5, 4°C, using a peristaltic pump. Eluted fractions were collected on ice in 1.5 ml tubes containing 150 µl of 1 M Tris pH 8.8 in order to neutralize the samples immediately. Protein concentration in the sample was determined by Bradford assay using BSA as a standard. Fractions of interest were pooled and transferred into PS buffer containing 150 mM KCl by repeated dilution and re-concentration in AmicomUltra-15 30 K ultrafiltration devices (Millipore). The antibodies were finally concentrated to 1–3 mg ml⁻¹, aliquoted, flash frozen in liquid nitrogen and kept at –20°C.

Papain digestion and Fab fragment purification. Antibody digestion with papain was described previously³⁶. In brief, 10 mg affinity-purified IgG were solubilized in 1 ml buffer A (150 mM NaCl, 1 mM EDTA, 25 mM mercaptoethanol, 10 mM NaP_i pH 7.3), 0.1 mg papain was then added and the mixture was incubated for 3 h at 37°C. 30 mM iodoacetamide was added to inhibit papain (15 min at 37°C). Afterwards, the sample was chilled to 4°C and loaded on a protein A agarose column (Pharmacia; 1.5 ml volume), which was pre-equilibrated with buffer B (100 mM KP_i, pH 8.0). The Fab-containing flow-through was dialysed against H₂O and concentrated by ultrafiltration through 30 kDa cut-off membranes (Millipore).

Purification of rVam7. Plasmid pGEX-KT::Vam7 (gift from A. Merz) was expressed in Rosetta 2 (DE3) (Novagen). Bacteria were grown in 2 l LB with 100 µg ml⁻¹ ampicillin and 25 µg ml⁻¹ chloramphenicol to OD_{600 nm} = 1, induced with 1 mM IPTG, 30°C for 4 h. Cells were collected and washed with PBSEEG (2 mM EDTA, 1 mM EGTA, 2 mM DTT, 1 mM PMSF in 1× PBS). The pellet was frozen in liquid nitrogen and stored at –80°C. For purification the sample was thawed, resuspended in 40 ml PBSEEG, sonicated twice (1 min on ice with maximal intensity), centrifuged (TI-60 rotor, 64,000 g, 30 min, 4°C) and the supernatant was incubated with 2–3 ml glutathione-sepharose 4B (GE Healthcare, 17-0756-01) under gentle rotation overnight at 4°C, and washed three or four times with PBSEEG. The resin was poured into a 10 ml polypropylene column (Thermo Scientific 2994) and washed with ten bed volumes of thrombin cleavage buffer (50 mM Tris-HCl pH 8.0, 100 mM NaCl, 2.5 mM CaCl₂, 0.1% β-mercaptoethanol) at room temperature. 200 U of thrombin (Sigma T-1063, 1000 U, dissolved in 0.5 ml thrombin cleavage buffer and 0.5 ml glycerol, aliquots had been kept at –20°C) were then added directly onto the column, the column was closed at both ends and incubated for 30 min at room temperature with end over end rotation. A second column with 1 ml *p*-aminobenzamide agarose (Sigma A-8332, 5 ml) was washed with 20 ml thrombin cleavage buffer. The glutathione-sepharose column was eluted with thrombin cleavage buffer applied directly onto this second column. Fractions of the flow-through were collected at the bottom of the second column. Protein levels were measured and fractions of interest were pooled. Eluted protein was transferred into PS buffer containing 150 mM KCl by repeated dilution and ultrafiltration in Amicom Ultra-15 30 K (Millipore), concentrated to a final 3 mg ml⁻¹, aliquoted, flash frozen in liquid nitrogen and kept at –20°C.

Purification of HOPS, HOPS subcomplexes and CORVET. These complexes were purified via the tandem affinity purification protocol, as previously

described³⁷. In brief, yeast cell lysates were prepared from 500 OD₆₀₀ equivalents of cells by thoroughly vortexing cells in lysis buffer (50 mM HEPES/KOH, pH 7.4, 300 mM NaCl, 0.15% NP-40 (Igepal CA-630, Sigma-Aldrich), 2 mM MgCl₂, 1 mM DTT, 1 mM PMSF and 1× FY protease inhibitor mix (Serva)) together with glass beads in a Disrupter Genie for 10 min at 2 °C, followed by centrifugation at 20,000g at 4 °C. The supernatant was centrifuged for 60 min at 100,000g, and the cleared lysate loaded onto 25 µl of prewashed IgG beads. After 1 h of incubation at 4 °C, the beads were washed three times with 1 ml lysis buffer containing 0.5 mM DTT, but lacking protease inhibitors. Bound proteins were eluted by tobacco etch virus protease (TEV) treatment for 1 h at 16 °C. TEV eluates were either analysed by SDS-PAGE and Coomassie staining or loaded onto 25 µl of prewashed calmodulin-sepharose beads, and incubated for 1 h at 4 °C. The beads were washed three times with 1 ml lysis buffer, bound proteins were eluted by incubation with 20 mM EGTA in lysis buffer for 20 min at 30 °C, analysed by SDS-PAGE and Coomassie staining and kept in small aliquots at -20 °C. Aliquots were thawed, and the proteins transferred into lysis buffer without DTT and NP-40 by repeated dilution and ultrafiltration (4 °C) in Amicon Ultra-15 30 K (Millipore). Re-concentrated proteins were used immediately for the experiment and not re-frozen.

Rapamycin-induced protein re-localization. Cells were grown in YPD overnight at 30 °C to early logarithmic phase. Cells were diluted to OD_{600 nm} = 0.2 for staining with 5 µM FM4-64 and then incubated with rapamycin (10 µM) before image acquisition.

Statistics for biological experiments. Where data were averaged, the samples stem from independent experiments with independent preparations of vacuoles or cells, that is, they represent biological replicates. Significance of differences has been evaluated through Student's *t*-test. Differences are only mentioned as such and interpreted if *P* < 0.005.

Molecular dynamics. Simulation model and settings. The molecular dynamics simulations were performed with the GROMACS v.4.5.7 simulation package³⁸. We used the MARTINI coarse-grained model^{39,40} to simulate the lipids, amino acids and solvent. In all simulations, the system was coupled to a constant temperature bath using the 'V-rescale' algorithm with a relaxation time of 1 ps. All simulations were performed at a temperature of 293 K. Periodic boundary conditions were applied to simulate bulk behaviour. The time step used in the simulation was 20 fs. The dielectric constant in the simulations was $\epsilon_r = 15$. The neighbour-list was updated every 10 simulation steps. The pressure was weakly coupled⁴¹ to 1 bar with a relaxation time of 1 ps. Here, only the *z* dimension was independently coupled to the pressure bath because the *x* and *y* dimensions of the simulation box were conserved (see 'Membrane simulation setups').

Modelling the vacuolar SNARE complex. The vacuole SNARE complex was modelled using the MARTINI model for proteins³⁹, which qualitatively captures the chemical nature of each individual amino acid and includes the secondary structure. For NYV1 the modelled sequence is "IGDATEDQKDVQIMNDNIDKFLERQERVSLVDKTSQNLSSSNKFRKAVNIKEIMWW[QKVKNI]ITLLTFTIILFVSAAFMFYLV", for VAM3: "TIIHQERSQQIGRIHTAVQEVNAIFHQGLGSLVKEQGEQVTTIDENISHLHDNMQANANKQLTRA[DQHQRDRNK]CGKVTLLIIHVCMVLLAVLS", for VTI1: "IDDDQRQQLLSNHAILKQSGDRDLKDSARIANETEGMSQIMMDLRSQRELENNARQTLFQADSYVDKSIKTLKTMTR[RLVANK]FISYAIIVLILLILLVLFKFKF", and for VAM7 "MQMVRDQEQLVALHRIQAQRGLALEMNEELQTQNELLALEDDVDNTGRRQLQIANKKARHF". Here, the square brackets enclose the defined juxta-membrane (linker) regions. The resolved and previously simulated structure⁴¹ of the neuronal SNARE complex was used as a template structure for the vacuolar SNARE complex. To this aim, we applied an external field, using a self-modified version of GROMACS, to drive the structure of the vacuole SNARE complex towards the known structure of the neuronal SNARE complex based on the known alignment. All residues are defined alpha-helical except for the defined SNARE linkers. The linkers are either modelled as a random coil '~' (in the case of unstructured) or alpha helical 'H' (in case of structured). We modelled all of the three SNARE linkers as being structured because such a scenario maximizes the force which a partly-assembled SNARE complex, by itself, can exert on the formed stalk.

Membrane simulation setups. In total, three different HOPS systems were simulated: (1) A system with three SNARE complexes (10,158 POPC, 6,771 POPE, 663,000 water molecules, dimension 48 × 64 × 37 nm³, *t*_{eq} = 1 µs), used in Fig. 4b and Extended Data Fig. 8); (2) a system with one SNARE complex (10,983 POPC, 400,000 water molecules, dimension 48 × 40 × 33 nm³, *t*_{eq} = 1 µs), used in Fig. 4a and Extended Data Figs 9b, 10); and (3) a system with one SNARE complex (13,621 POPC, 500,000 water molecules, dimension 67 × 40 × 40 nm³, *t*_{eq} = 2 µs), used in Fig. 4a and Extended Data Fig. 9b. For studying the fusion pore, the system was made slightly larger in order to avoid the fusion pore and the free membrane edges becoming too close (see the paragraph below).

It is important to emphasize that the two opposing membranes must be able to freely adopt their (local) separation distance in order to realistically mimic a

scenario in which two vacuoles fuse. To this aim, we cut the periodicity of the membrane along the *x* dimension (thus preventing solvent becoming 'trapped' in the space between the two opposing leaflets). The latter creates four free membrane edges (for example, see Extended Data Fig. 8) that facilitate rapid flip-flop between the leaflets and thereby ensure that the spontaneous curvature of the membrane vanishes when the membrane is bent (preventing finite-size effects). Furthermore, the ability to adapt freely the area of the membrane ensures that the membrane minimizes its shape under tensionless conditions in the presence of HOPS and thus the work performed by HOPS is only determined by membrane bending energy. Finally, to prevent the large line tension of the free membrane edges strongly deforming the simulation box (it prefers to minimize the *y* dimension while maximizing the *x* dimension) the *x* and *y* dimensions of the simulation box were kept constant. Hence, pressure coupling along these dimensions is redundant for a membrane cut in one dimension because the membrane area can independently adjust with respect to the (corresponding) area of the simulation box (the system is isotropic).

Model and setup of the HOPS simulations. In our simulations, 'soluble' HOPS is modelled by a soft harmonic repulsive potential ($K_{\text{force}} = 50 \text{ kJ nm}^{-2} \text{ mol}^{-1}$). The 'attractive' HOPS is modelled by the potential function, $V(d) = K_{\text{force}} d^2 (d^2 - C)$, where $V(d)$ is the potential energy as a function of the penetration depth (*d*), that is, the distance beyond the surface of HOPS. Here, K_{force} and *C* (the width of the well) are set to $K_{\text{force}} = 20 \text{ kJ nm}^{-2} \text{ mol}^{-1}$ and $C = 0.4 \text{ nm}^2$. Because the additional presence of attractions reduces the apparent radius of HOPS, we compensated for this by slightly increasing its radius (7.4 nm versus 7.0 nm). The HOPS potential only acted on the carbon tails and glycerol parts of the lipids. To mimic a SNARE complex that is slightly embedded by HOPS¹¹, we modelled a slight overlap between HOPS and the SNARE complex, that is, the SNARE complex was located within HOPS about 2 nm away from its surface (see Extended Data Figs 8 and 10). In reality, the depletion of solvent interactions upon binding will be compensated by competitive interactions with the binding pocket of HOPS. In our model, solvent was allowed to freely enter and pass HOPS in order to conserve ongoing interactions within the coiled-coil complex of the SNAREs. The main advantage of modelling HOPS by an effective potential is that this allows direct quantification of the work which HOPS must perform to conserve the corresponding membrane shape of minimal free energy. The HOPS simulations were set up via the slow growth method, that is, the radius of HOPS was gradually increased from 0 to the target radius over 80 ns. During this procedure, the SNARE complex was restrained by restraining only a single bead within the SNARE complex (the backbone bead of residue Gly218 within Vam3) via a harmonic potential ($K_{\text{force}} = 1000 \text{ kJ nm}^{-2} \text{ mol}^{-1}$). After equilibrium was reached—equilibrium was characterized by the pressure (bending work) and the resultant force on HOPS—we restrained 15 additional backbone atoms within Vam3 (Gly218–Asp232) to simulate a torsional restraining effect of the binding pocket on the SNARE complex.

Finally, the stalk in all of the setups is generated by applying an external field. Here, we applied a harmonic potential ($50 \text{ kJ nm}^{-2} \text{ mol}^{-1}$) to induce a cylindrically shaped void of 1 nm radius in the solvent layer between the bilayers. The hydrophobic nature of the void attracts the lipid tails in the adjacent leaflets and results in the formation of a stalk. Notably, this whole process occurs on a timescale of only a few nanoseconds. The external potential is removed before subsequent equilibration and introduction of the HOPS sphere.

Free energy of fusion and SNARE forces. We performed two different types of so-called umbrella sampling protocols with different goals: (1) How does HOPS binding affect the free energy landscape of fusion pore opening? To answer this question, we used simulation system 1 (see above) with probe to probe distance (stalk thickness) as a reaction coordinate. (2) How does HOPS binding affect the force that the bound SNARE complex exerts on a fusion intermediate? To answer this question, we used simulation system 2 (see above) with the distance between the C termini of Nyv1 and Vam3 as a reaction coordinate.

In protocol 1, we pull two hydrophilic beads (probes) through the stalk centre in order to estimate the free energy required to open the fusion pore. Each probe consists of 8 clustered solvent beads. The 'stalk thickness' is defined by the distance between the two probes. The rationale is to bring the system close to the nucleation barrier until that barrier can be crossed spontaneously within the simulation time scales. The work required to enforce nucleation provides an estimate of the height of the barrier. For more detailed information see our previous work³².

In protocol 2, we study how HOPS binding alters the force that the C termini of Nyv1 and Vam3 exert on the stalk intermediate. We infer such an effect from the relative change in work required to slightly pull the SNARE C termini (Nyv1 and Vam3) in closer proximity in the presence or absence of HOPS. 'Slightly' here implies that we only indent/squeeze the stalk such that the stalk will recover if an active pulling force is no longer applied (thermodynamically reversible).

To derive the associated free energies in both of these protocols, we applied umbrella simulation techniques ($K_{\text{force}} = 1000 \text{ kJ nm}^{-2} \text{ mol}^{-1}$) in combination with

the weighted histogram method. We generated independent states along the reaction coordinate (50 for protocol 1, 15 for protocol 2) by performing a stirred molecular dynamics simulation over the entire reaction coordinate (pull rate: $-5 \times 10^{-5} \text{ nm ps}^{-1}$) in a pre-equilibrated system. Equilibrium was characterized by the pressure (bending work) and the resultant force on HOPS. For protocol 1, a separate, independent stirred molecular dynamics run must be performed for each different system (for example, the attractive HOPS case) because the generated states will embed information about the nature of the barrier. The umbrella simulations were performed after the systems were equilibrated for $\sim 1.6 \mu\text{s}$, that is, the last snapshot was used for a stirred molecular dynamics simulation, from which the different umbrella windows were generated. Equilibrium was characterized by the pressure (bending work) and the resultant force on HOPS. Each umbrella window was simulated over an effective time of 400–600 ns to obtain overlapping distributions from which the total free energy profile was constructed. We discarded the first 40 ns of the simulation to ensure equilibration of the measured biased force. All of the free energy profiles and error bars therein were obtained by using the WHAM method in combination with the Bayesian bootstrapping method⁴². The bootstrapping method exploits the WHAM equations to reconstruct a large number of free energy profiles from re-sampled bootstrap histograms. The errors within the final free energy profile are estimated from the statistical fluctuations. Each re-sampled histogram of the biased force is reconstructed from the data which comprise the original histogram (an umbrella window) by random selection with replacement. This resampling procedure respects the integrated autocorrelation time (estimated on the fly) within the biasing force and adds an additional random weight to the histogram within the WHAM equations (Bayesian bootstrapping). A detailed description of this procedure has been previously published⁴².

Bending energy and force. The bending work is estimated from the total (equilibrium) force that the membrane exerts on the surface of HOPS after it adopts its shape of minimal free energy. The work (W_{eq}) that HOPS must perform to bend the membrane is given by the relationship $W_{\text{eq}} = 1/3 \sum f_{\text{eq},av} r$, where $\sum f_{\text{eq},av}$ is the total average force that acts on the surface of the HOPS sphere during growth from radius $r=0$ to $r=r$. Our continuum elastic calculations revealed that $\sum f_{\text{eq}}$ linearly increases with r . Therefore, we approximated $\sum f_{\text{eq},av}$ from $r=0$ to $r=r$ by $1/2 \sum f_{\text{eq}}$ at $r=r$. This linear approximation enables instantaneous calculation of W_{eq} by averaging over a single simulation (at $r=r$). For a purely repulsive sphere these relationships approximate the concomitant bending energy of the adopted membrane shape. We expect, however, to slightly systematically overestimate the bending energy (by a few $k_{\text{B}}T$) since the force on the HOPS sphere will in reality vanish slightly before $r=0$ ($r \approx 0.5 \text{ nm}$). This is due to the approximately 1 nm inter-membrane separation resulting from the presence of the stalk. Notably, HOPS bends the membrane by actively pressing against the membrane surface (indentation). This additional stress term (for example, thinning of the membrane) is omitted within the Hamiltonian of the continuum model but is not expected to largely contribute to the surface free energy. The peristaltic force (f_{a}) on HOPS (see Extended Data Fig. 9) is calculated by projecting the resultant force on HOPS (a 3-vector) on the vector connecting the centre of HOPS with the stalk centre. Here, the stalk centre is defined as the geometrical centre between the C terminus of Nyl1 and Vam3. Finally, the average values of bending work and f_{a} are obtained by averaging over 1–2 μs equilibrium simulations. The error in the average value is obtained by block averaging.

Continuum model. Continuum models were performed by minimizing the Helfrich Hamiltonian within the de Monge representation $z(x,y)$ subjected to two constraints: (1) the inter-membrane constraint (a stalk or partly-assembled SNARE complex), and (2) a solid sphere (HOPS). The membrane was described by a discretized sheet consisting of 100 grid elements in the y dimension, and 200 in the x dimension. For reasons of symmetry, we only model one-quarter of the actual system and recover the full surface free energy by multiplication by a factor of four (for the projected area by a factor of two). Reflecting boundary conditions were used in the y dimension (the symmetry axis), periodic in the x dimension. The actual membrane contact surface in vacuole fusion is of microscopic dimension^{43–45}, indicating that a large multiple of constraints must be present and that the membrane is not ‘free standing’ even over large distances. All dimensions are based on the positions of the C4 lipid tail beads (the mid-plane of the membrane) within the molecular dynamics simulations. Finally, HOPS embeds the SNARE complex non-symmetrically¹¹ and will therefore induce torque. Torque (a three body force) does not occur when the distance (d) between the centre of HOPS and the stalk (the two constraints) is used as a reaction coordinate but can be additionally derived or constructed by scaling f_{a} with a $\sin(\theta)$ term.

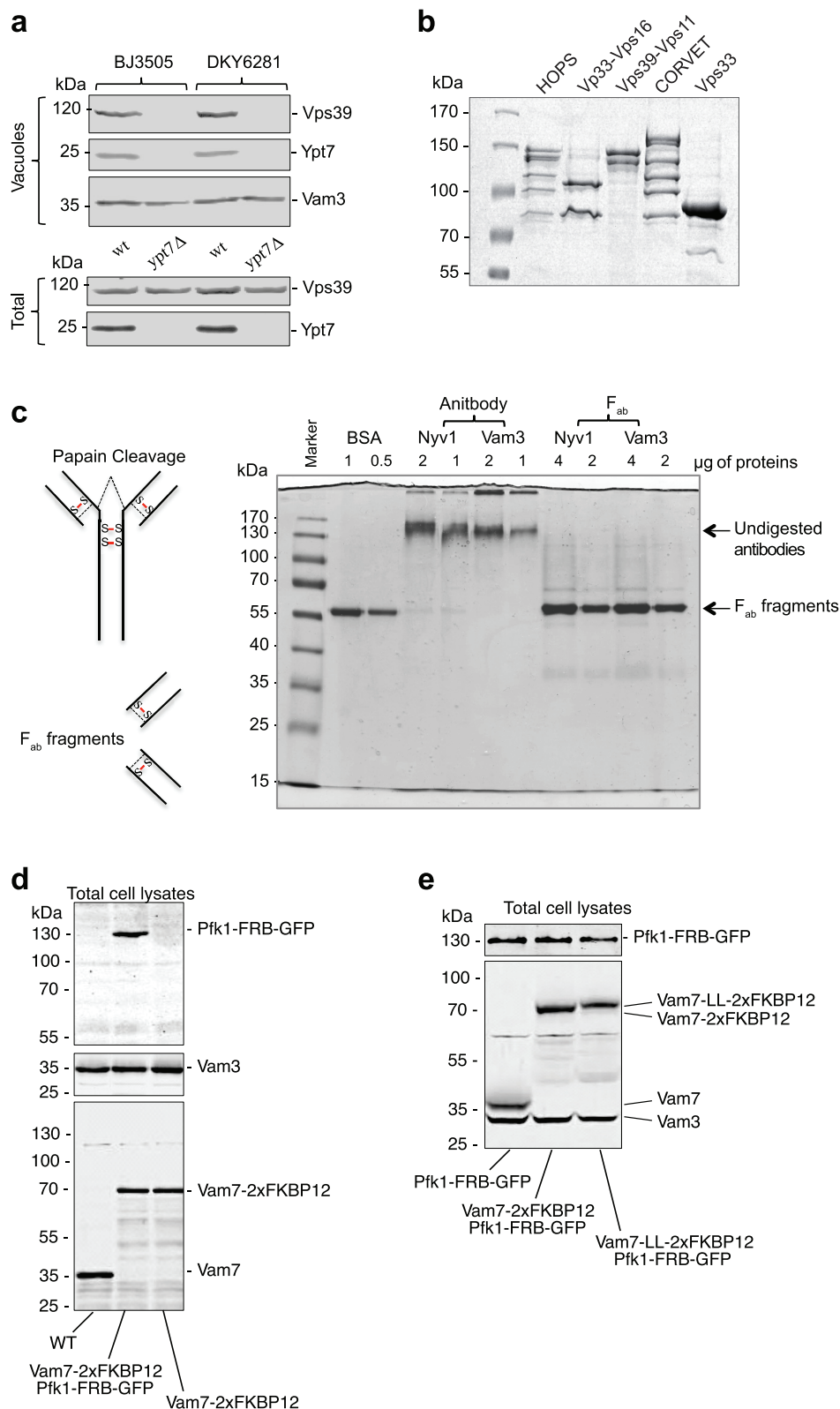
The Hamiltonian for each surface element, F_{total} , is given by $F_{\text{bending}} + F_{\text{constraint}} + F_{\text{HOPS}}$, with F_{bending} being the Helfrich bending energy, $F_{\text{constraint}}$ the energy of the inter-membrane constraint (a stalk, fusion pore or partly assembled SNARE complex) and F_{HOPS} the energy of the HOPS sphere. F_{bending} is given by $2\kappa H^2$ with H being the mean curvature, and κ the bending modulus

($24 k_{\text{B}}T$, see ref. 9). The constraint $F_{\text{constraint}}$ is modelled by a set of stiff springs which restrains the membrane at a height of $z_{\text{equ}} = 2 \text{ nm}$ and which imposes a circular ‘stalk’ region with a radius of $d_{\text{stalk}} = 2 \text{ nm}$. $F_{\text{constraint}}$ depends on the distance (d) between a surface element and the centre of the ‘stalk’ region, and the height of the membrane z . $F_{\text{constraint}} = 0$ if $d > 2 \text{ nm}$ and $1/2K_{\text{stalk}}(z - z_{\text{equ}})^2(d - d_{\text{stalk}})$ otherwise, with K_{stalk} being the force constant, $K_{\text{stalk}} = 100 k_{\text{B}}T \text{ nm}^{-5}$. Here, the term $(d - d_{\text{stalk}})$ ensures a smooth (differentiable) transition of the ‘stalk’ region. HOPS was modelled as a sphere with a diameter D_{H} . The centre of the sphere is located within the x - y plane at $z = 0$. Surface elements overlapping with the HOPS sphere experience an harmonic repulsion, $F_{\text{HOPS}} = 1/2K_{\text{HOPS}}(2r - D_{\text{H}})^2$ if $2r < D_{\text{H}}$ and $F_{\text{HOPS}} = 0$ otherwise, with r being the distance of a surface element from the centre of the sphere. The force constant K_{HOPS} was chosen to be $100 k_{\text{B}}T \text{ nm}^{-4}$. The example of a (moderately) attractive HOPS was modelled using $F_{\text{HOPS}} = K_{\text{HOPS}}d^2(d^2 - C)$ with $C = 0.5 \text{ nm}^2$, and $K_{\text{HOPS}} = 20 k_{\text{B}}T \text{ nm}^{-6}$. Finally, the total surface free energy $\sum F_{\text{total}}dA$ was minimized using an over-damped deterministic minimization scheme. We emphasize that the values predicted by the continuum model are subject to the simplification of the characteristics of the system (for example, exact spatial dimensions, and the nature of the inter-membrane restraint). They also rely on the estimation of the bending modulus of the membrane.

Code availability. The molecular dynamics simulations were performed with a self-modified version of the open source software GROMACS v4.5.5. The implementation of the HOPS potentials used here is described in detail in the Supplementary Information. The code is publicly available at <http://nlr.theorie.physik.uni-goettingen.de/~hrissel/code/>

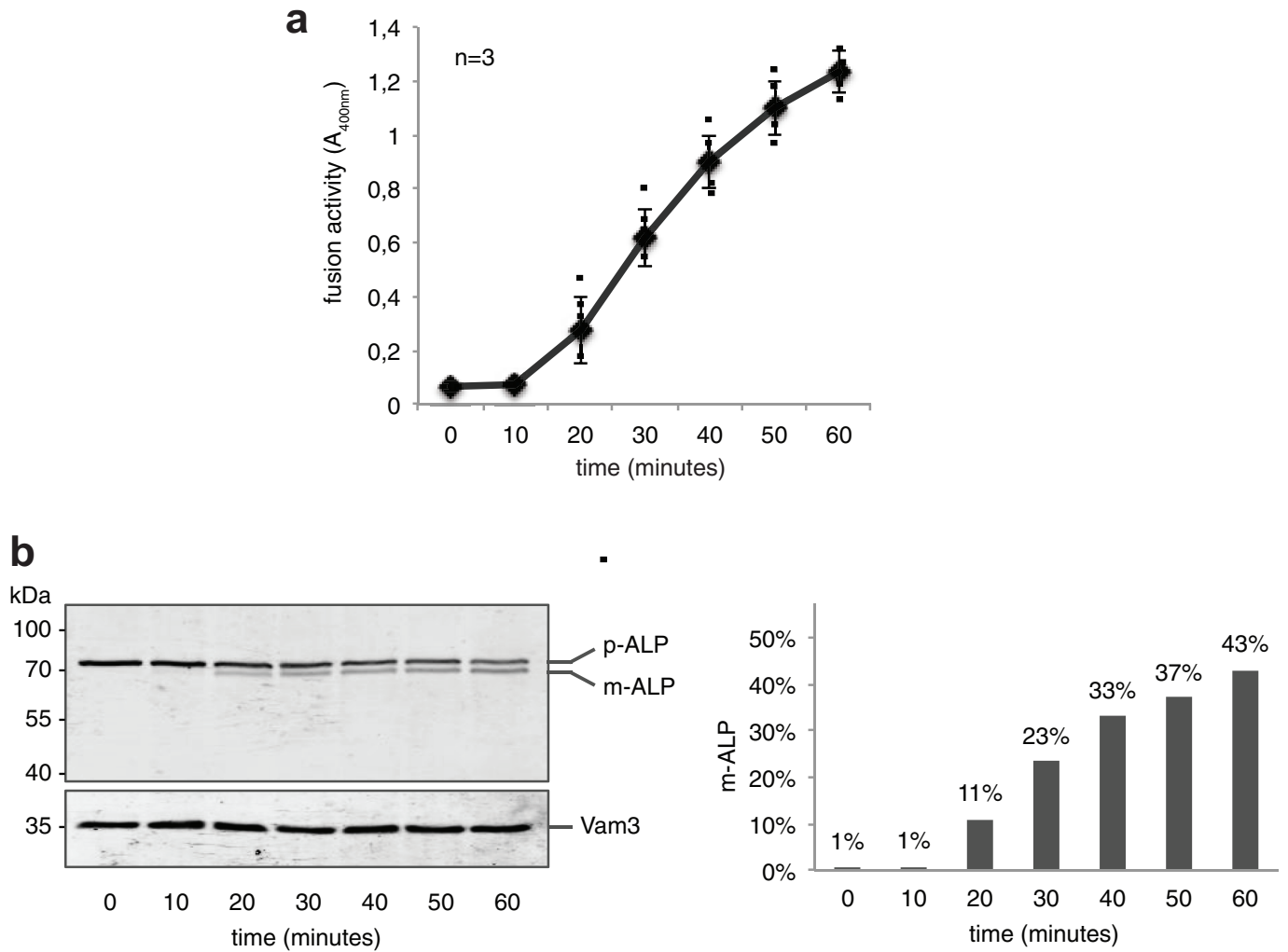
Data availability. All original data will be made available by the corresponding authors upon reasonable request. For gel source data, see Supplementary Fig. 1. Source Data for Fig. 1d, e is available online.

- Janke, C. *et al.* A versatile toolbox for PCR-based tagging of yeast genes: new fluorescent proteins, more markers and promoter substitution cassettes. *Yeast* **21**, 947–962 (2004).
- Longtine, M. S. *et al.* Additional modules for versatile and economical PCR-based gene deletion and modification in *Saccharomyces cerevisiae*. *Yeast* **14**, 953–961 (1998).
- Kuznetsova, I. M., Turoverov, K. K. & Uversky, V. N. What macromolecular crowding can do to a protein. *Int. J. Mol. Sci.* **15**, 23090–23140 (2014).
- Mage, M. G. in *Immunochemical Techniques* Vol. 70 (eds Vunakis, H. V. & Langone, J.) 142–150 (Elsevier, 1980).
- Ostrowicz, C. W. *et al.* Defined subunit arrangement and Rab interactions are required for functionality of the HOPS tethering complex. *Traffic* **11**, 1334–1346 (2010).
- Hess, B., Kutzner, C., van der Spoel, D. & Lindahl, E. GROMACS 4: algorithms for highly efficient, load-balanced, and scalable molecular simulation. *J. Chem. Theory Comput.* **4**, 435–447 (2008).
- Monticelli, L. *et al.* The MARTINI coarse-grained force field: extension to proteins. *J. Chem. Theory Comput.* **4**, 819–834 (2008).
- Marrink, S. J., Risselada, H. J., Yefimov, S., Tieleman, D. P. & de Vries, A. H. The MARTINI force field: coarse grained model for biomolecular simulations. *J. Phys. Chem. B* **111**, 7812–7824 (2007).
- Risselada, H. J., Kutzner, C. & Grubmüller, H. Caught in the act: visualization of SNARE-mediated fusion events in molecular detail. *ChemBioChem* **12**, 1049–1055 (2011).
- Hub, J. S., De Groot, B. L. & van der Spoel, D. g_wham—a free weighted histogram analysis implementation including robust error and autocorrelation estimates. *J. Chem. Theory Comput.* **6**, 3713–3720 (2010).
- Mayer, A. & Wickner, W. Docking of yeast vacuoles is catalyzed by the Ras-like GTPase Ypt7p after symmetric priming by Sec18p (NSF). *J. Cell Biol.* **136**, 307–317 (1997).
- Wang, L., Merz, A. J., Collins, K. M. & Wickner, W. Hierarchy of protein assembly at the vertex ring domain for yeast vacuole docking and fusion. *J. Cell Biol.* **160**, 365–374 (2003).
- Karunakaran, S., Sasser, T., Rajalekshmi, S. & Fratti, R. A. SNAREs, HOPS and regulatory lipids control the dynamics of vacuolar actin during homotypic fusion in *S. cerevisiae*. *J. Cell Sci.* **125**, 1683–1692 (2012).
- Merz, A. J. & Wickner, W. T. Resolution of organelle docking and fusion kinetics in a cell-free assay. *Proc. Natl. Acad. Sci. USA* **101**, 11548–11553 (2004).
- Lürrick, A. *et al.* Multivalent Rab interactions determine tether-mediated membrane fusion. *Mol. Biol. Cell* **28**, 322–332 (2016).
- Jackson, M. B. Minimum membrane bending energies of fusion pores. *J. Membr. Biol.* **231**, 101–115 (2009).
- Ryham, R. J., Ward, M. A. & Cohen, F. S. Teardrop shapes minimize bending energy of fusion pores connecting planar bilayers. *Phys. Rev. E* **88**, 062701 (2013).
- D’Agostino, M., Risselada, H. J. & Mayer, A. Steric hindrance of SNARE transmembrane domain organization impairs the hemifusion-to-fusion transition. *EMBO Rep.* **17**, 1590–1608 (2016).
- Pieren, M., Desfougères, Y., Michailat, L., Schmidt, A. & Mayer, A. Vacuolar SNARE protein transmembrane domains serve as nonspecific membrane anchors with unequal roles in lipid mixing. *J. Biol. Chem.* **290**, 12821–12832 (2015).



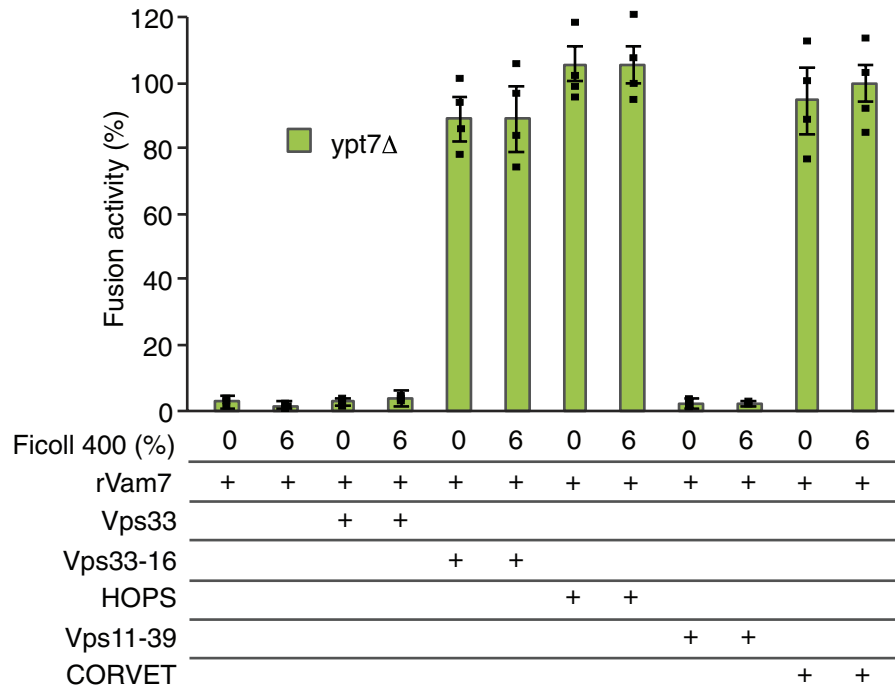
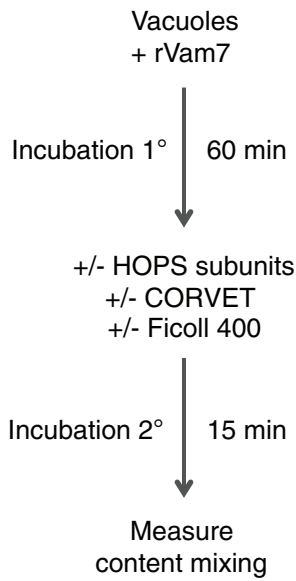
Extended Data Figure 1 | Optimization and production of reaction components. **a**, *ypt7* Δ vacuoles lack HOPS. Ypt7 and HOPS content of total cell extracts and purified vacuoles from wild-type and *ypt7* Δ mutants in BJ3505 and DKY6281 cells, representing the background strains used for the content mixing assay. **b**, Purified HOPS, HOPS subcomplexes and CORVET. The complexes used for the *in vitro* experiments were analysed by SDS-PAGE and Coomassie staining. The gel represents the preparations, which followed published routine procedure, used for the experiments in Fig. 1 and Extended Data Figs 3 and 4. **c**, Production of Fab fragments from polyclonal antibodies to Vam3 and Nyv1. Schematic

view of papain cleavage sites for Fab fragment generation (left). Affinity-purified antibodies and Fab fragments extracted after papain digestion were analysed by non-reducing SDS-PAGE and Coomassie staining. The gel shows the preparation used in Fig. 2. **d**, Expression of FKBP and FRB fusion proteins. Total cell extracts were prepared from 0.1 OD_{600 nm} units of logarithmic cultures of yeast strains expressing Vam7-2 \times FKBP12 and/or Pfk1-FRB-GFP. Proteins were analysed by SDS-PAGE and western blotting against Vam7, Vam3 and GFP. **e**, As in **d**, but for cells expressing Vam7-LL-2 \times FKBP12, containing the 35-amino-acid linker. For **a** and **c-e**, similar results were obtained from two independent preparations.



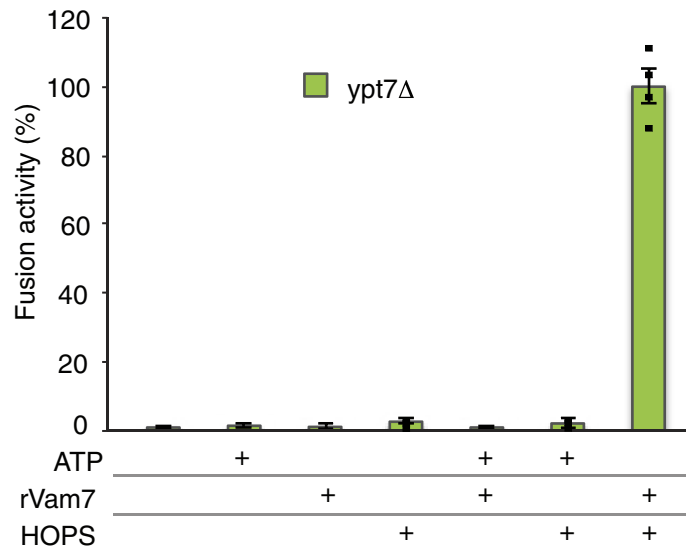
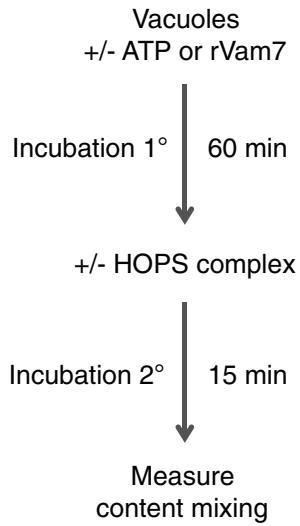
Extended Data Figure 2 | Kinetics and efficiency of *in vitro* vacuole fusion, measured by content mixing. Vacuoles were prepared from two different strains, which contain either the soluble 45-kDa maturase Pep4 (contained in DKY6281) or the pro-alkaline phosphatase (p-ALP) (contained in BJ3505). Formation of a sufficiently large fusion pore allows Pep4 to transfer into the p-ALP containing fusion partner, leading to proteolytic cleavage of its pro-sequence and activation of the enzyme (m-ALP). This activity is used as a measurement of fusion. Note that proteolytic maturation of p-ALP is fast and not limiting for the development of the content mixing signal⁴⁶. Standard fusion reactions were started, and aliquots were withdrawn at the indicated time points

and set on ice. **a**, At the end of the 60 min period, m-ALP activity was determined for all samples. Data are means \pm s.d. from 3 biologically independent experiments. **b**, Aliquots from one of the experiments in (a) were trichloroacetic acid (TCA)-precipitated and analysed by SDS-PAGE and western blotting against ALP and Vam3. Signals were detected on a LICOR infrared scanner (left) and quantified (right) as the ratio of m-ALP to (m-ALP + p-ALP). Vam3 has been included as a loading control. Note that after one round of fusion, only a maximum of 50% of p-ALP can be matured, because half of the fusion events in the suspension will occur between like vacuoles (that is, Pep4/Pep4 or p-ALP/p-ALP) and will not produce a signal.



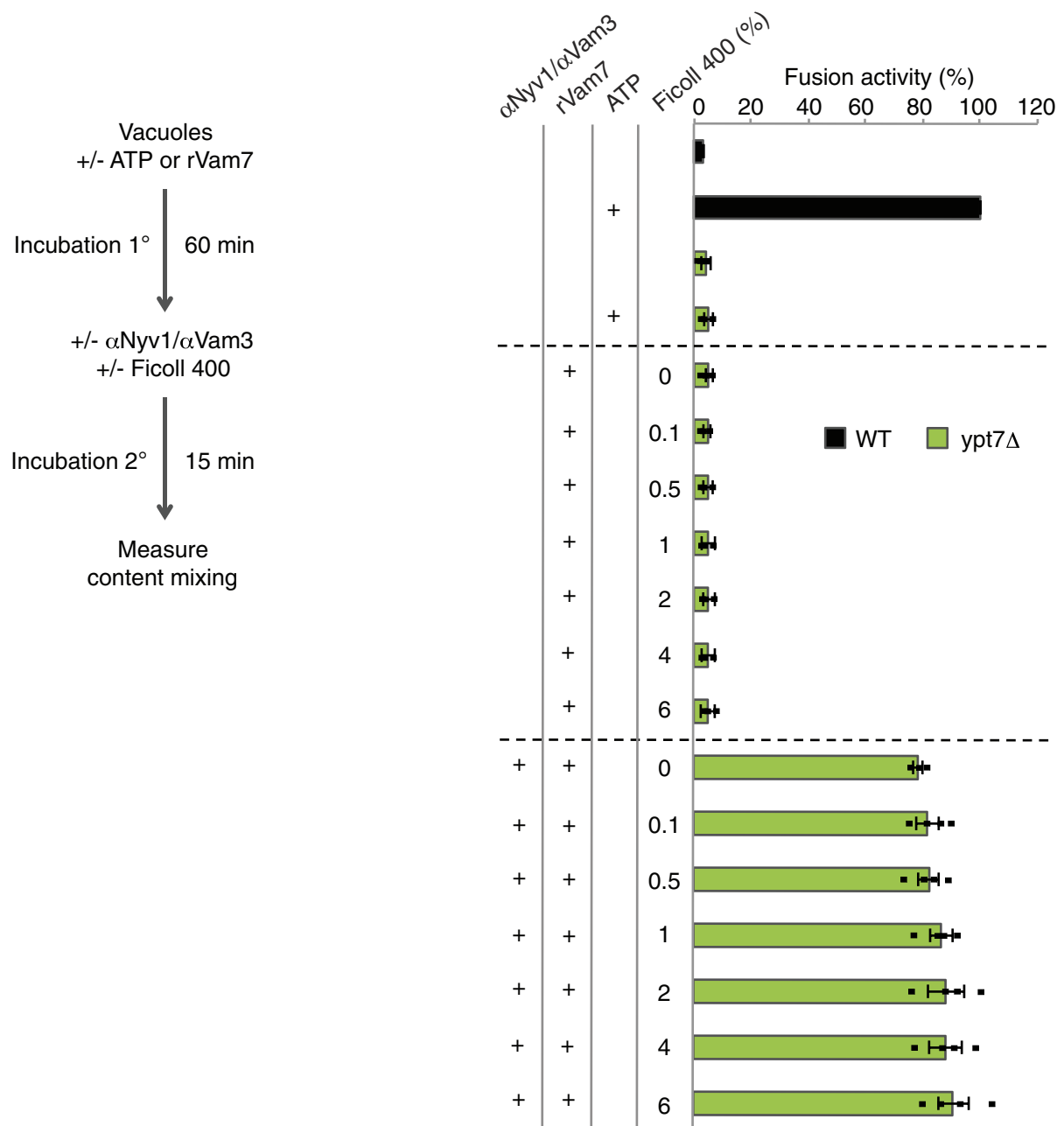
Extended Data Figure 3 | HOPS and CORVET complexes stimulate fusion to similar degrees. Two-stage fusion reactions with *ypt7Δ* vacuoles were run as in Fig. 1g, in the absence of ATP. rVam7 had been added in the first phase of the incubation (1°), and either 0.4 μM HOPS subcomplexes or 0.4 μM CORVET was added during the second incubation (2°). Half of the samples also received 6% Ficoll-400, an agent mimicking molecular

crowding³⁵, during the second incubation. At the end of the 75-min incubation period, content mixing was assayed. Fusion activity of a standard wild-type reaction performed in the presence of ATP served as a 100% reference. Data are mean ± s.d. from 3 biologically independent experiments.



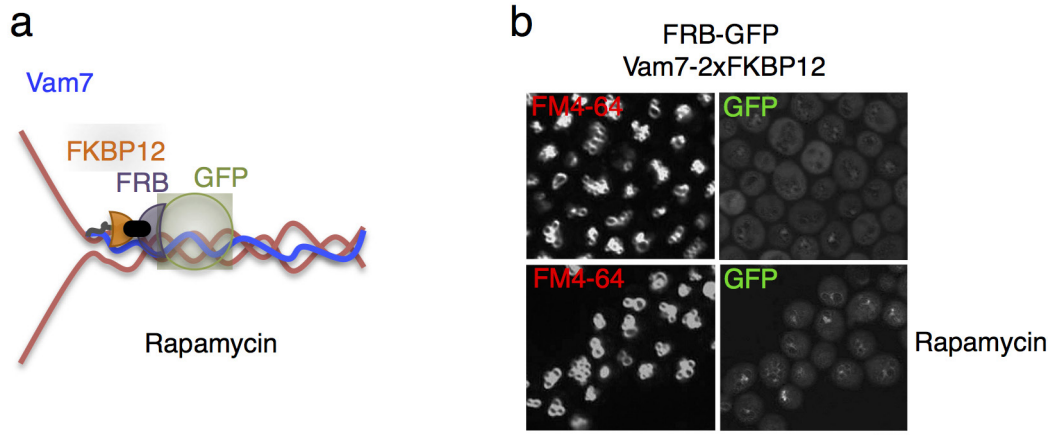
Extended Data Figure 4 | *ypt7Δ* vacuoles require both Vam7 and HOPS for content mixing. Two-stage fusion reactions were run as in Fig. 1g in the presence or absence of ATP. rVam7 was added in the first phase of the

incubation, HOPS was added only in the only in the second incubation. At the end of the 75-min incubation period, content mixing was assayed. Data are mean ± s.d. from 3 biologically independent experiments.



Extended Data Figure 5 | A molecular crowding agent cannot stimulate fusion in the absence of bulky SNARE ligands. Two-stage fusion reactions with *ypt7 Δ* vacuoles were run as in Fig. 2b, in the absence or presence of ATP. rVam7 was added in the first phase of the incubation where indicated, antibodies and various concentrations of the crowding

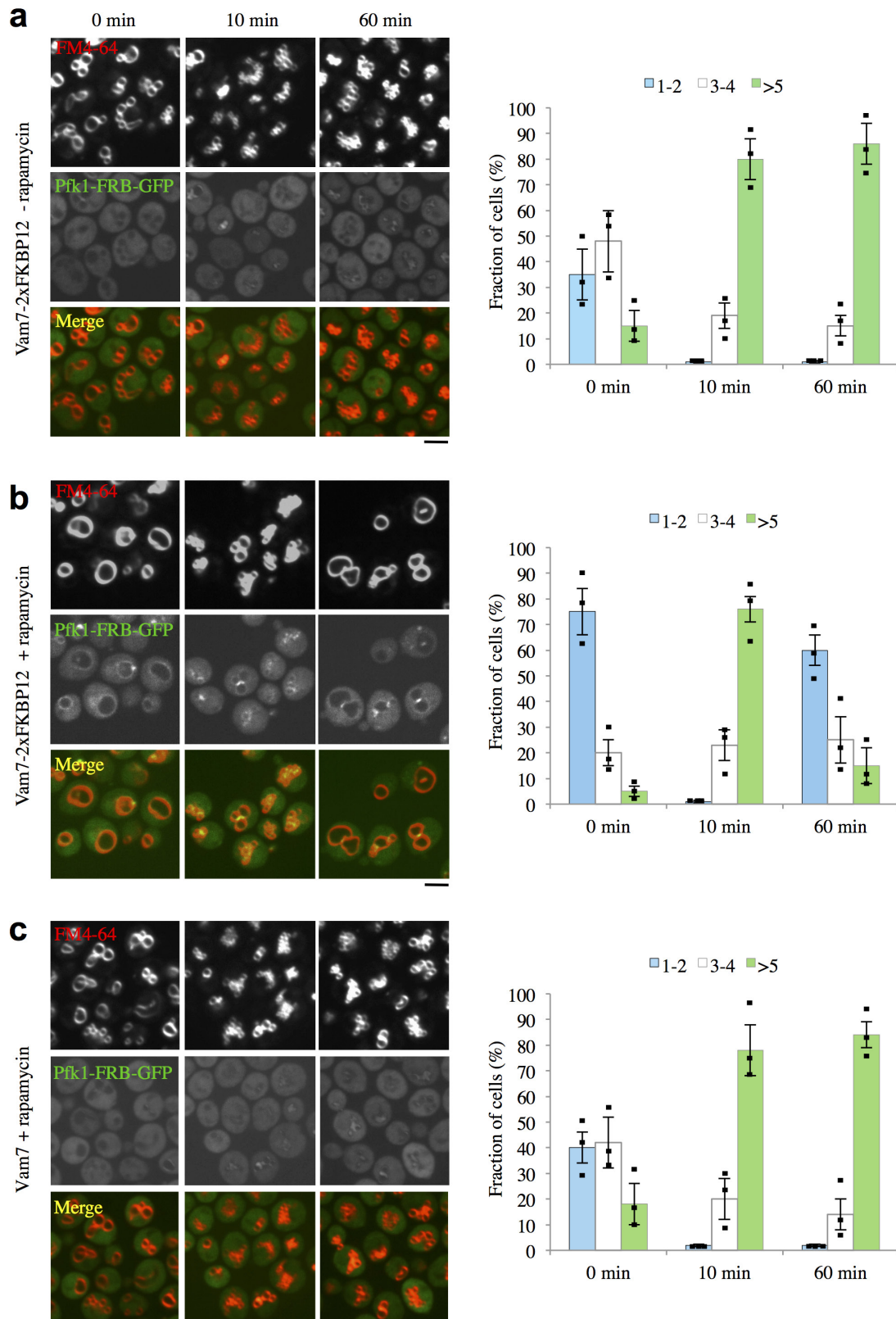
agent Ficoll-400 were added only during the second incubation. At the end of the 75-min incubation period, content mixing was assayed. Fusion activity of a wild-type reaction performed in the presence of ATP served as a 100% reference. Data are mean \pm s.d. from 3 biologically independent experiments.



Extended Data Figure 6 | Effect of rapamycin-induced dimerization on *in vivo* vacuole fusion using the small fusion protein FRB-GFP.

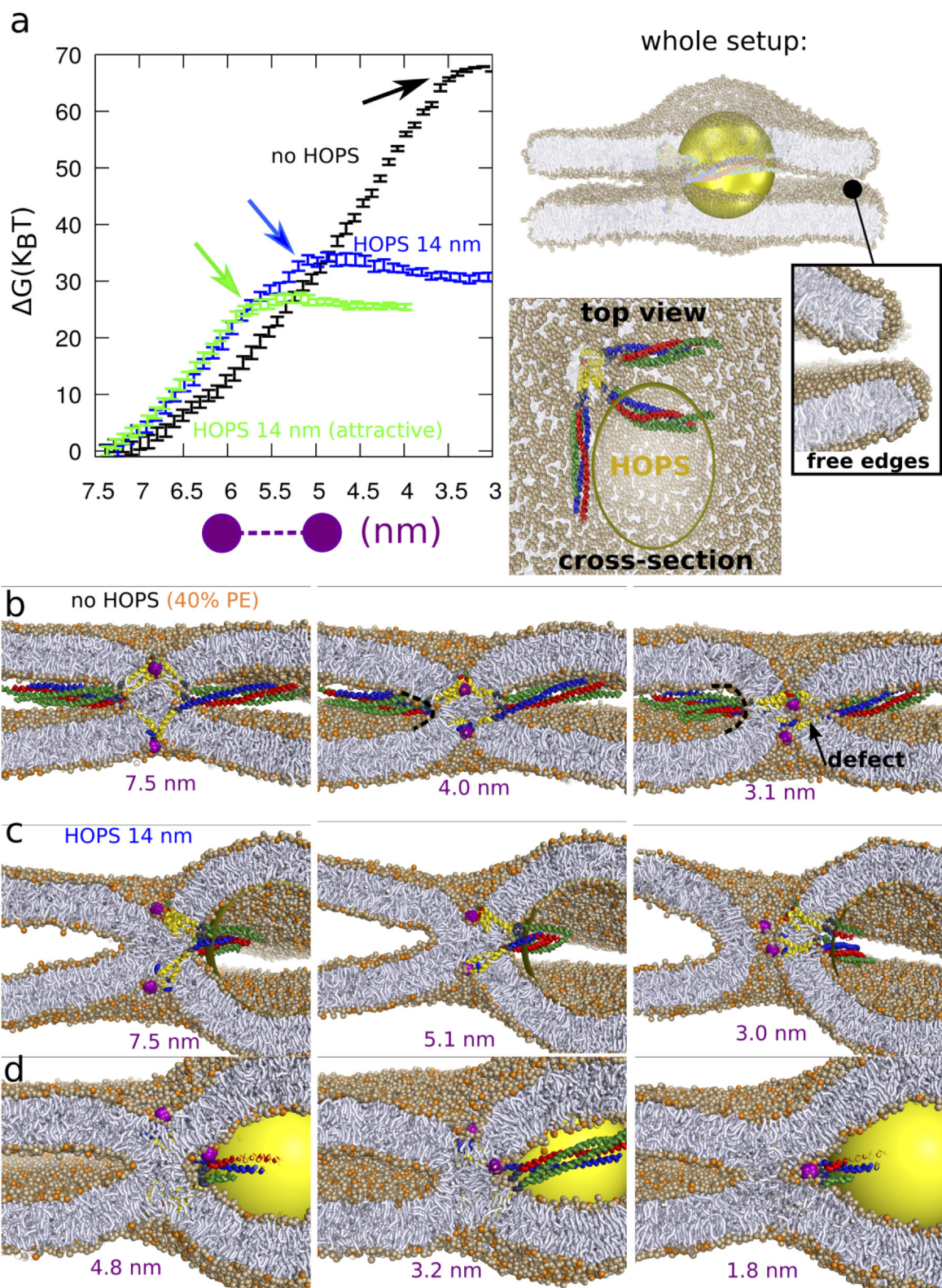
a, Schematic view of rapamycin-induced FKBP12/FRB-tagged protein dimerization between Vam7-2×FKBP12 and FRB-GFP.
b, Logarithmically growing cells, expressing tagged Vam7-2×FKBP12,

were stained with the vacuole tracer FM4-64 and analysed by spinning disc microscopy before and 10 min after the addition of 10 μM rapamycin. Scale bar, 5 μm. Similar results were obtained in 3 biologically independent repetitions.



Extended Data Figure 7 | Fusion can be prematurely triggered by protein recruitment after osmotically induced vacuole fragmentation.
a, Logarithmically growing cells, carrying Vam7-2xFKBP12 and Pfk1-FRB-GFP as indicated, were stained with the vacuole tracer FM4-64. Vacuole fission was induced by adding 0.5 M NaCl. Cells were analysed by spinning disc microscopy before and 10 and 60 min after salt

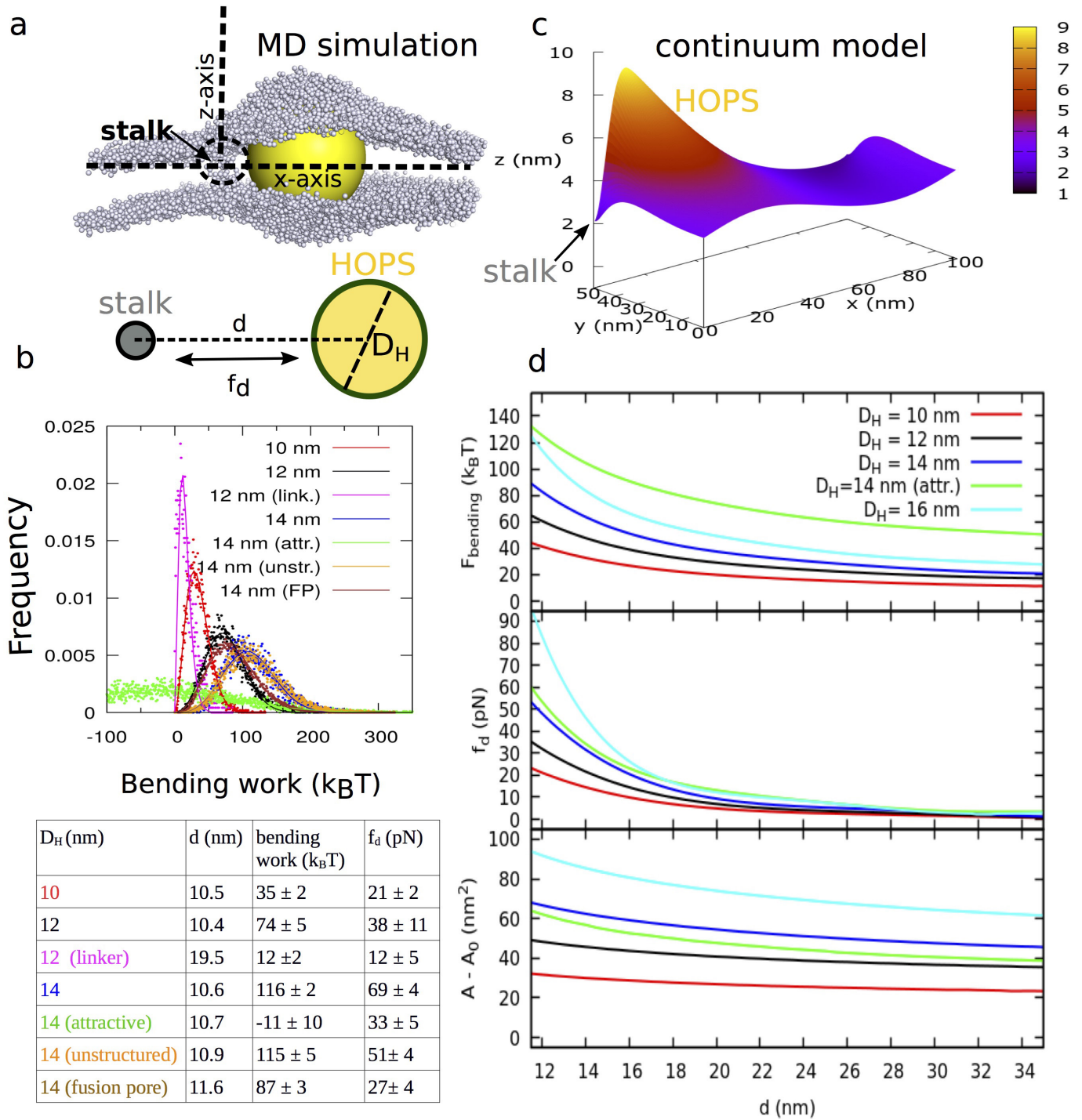
addition. The cells were grouped into three categories according to the number of vacuoles visible per cell. 100 cells were analysed per sample.
b, As in **a**, but 10 μ M rapamycin was added before the salt shock. **c**, As in **b**, but with cells expressing non-tagged Vam7. Data are mean \pm s.d. from 3 biologically independent experiments. Scale bars, 5 μ m.



Extended Data Figure 8 | See next page for caption.

Extended Data Figure 8 | Effect of HOPS on the free energy barrier of fusion pore formation. This plot complements Fig. 4. **a**, The free energy barrier of fusion pore opening is derived for a simulated system consisting of three SNARE complexes (right) and a POPC membrane that contains 40% POPE (coloured orange). To this aim, we pull two hydrophilic probes (coloured purple) towards the centre of the stalk and estimate the work (ΔG) as a function of probe–probe distance (the stalk thickness)³². The arrows in the free energy profile indicate the nucleation barrier for the fusion pore. Beyond this stage, subsequent pore opening proceeds in the absence of additional work (the plateau region). Tethering complexes such as HOPS are attracted to the membrane by Rab-GTPases or through direct lipid interaction^{10,47}. An attractive HOPS surface (green line) conserves the lowered nucleation barrier, even when the surface attractions fully compensate the membrane bending energy (no net bending work; Extended Data Fig. 9). Error bars are calculated via Bayesian resampling of 50 overlapping WHAM histograms⁴² Each parental WHAM

histogram consists of more than 30,000 data points (autocorrelation up to approximately 1,500 data points). **b**, Pore formation in the absence of HOPS. A defect is frequently formed in the vicinity of the SNARE TMDs (black arrow), illustrating the presence of a high stress (the defect probably decreases the bending stress). Fusion pore formation is associated with a sudden reduction of the sharp curvature near the circumference of the stalk (dashed lines). Fusion pores tend to adopt a teardrop shape^{48,49}. **c**, Fusion pore formation in the presence of HOPS. The pre-existing teardrop membrane shape imposed by HOPS likely provides a geometrical and therefore an energetic advantage for pore formation. **d**, Set up in which we artificially enforced formation of a leakage pore/defect in the direct vicinity of the stalk (the rationale behind this has been previously explained³²). The induced defect (between 3.2 and 1.8 nm the probe pierced through the membrane) instantaneously recovers. This suggests that the stress that HOPS imposes on the fusion site does not prime fusion to become leaky.

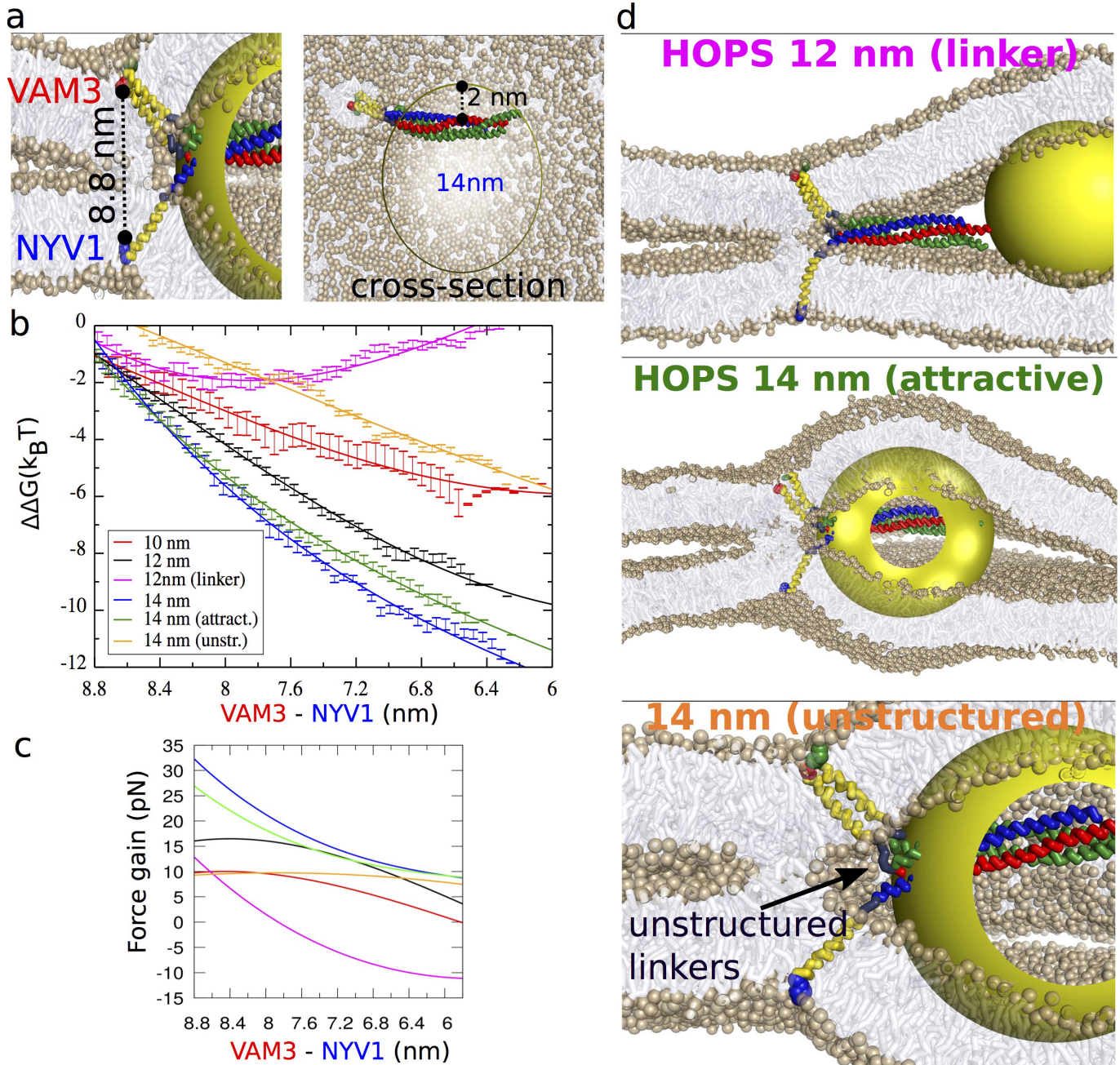


Extended Data Figure 9 | See next page for caption.

Extended Data Figure 9 | Detailed analysis of HOPS-mediated membrane bending in the presence of an inter-membrane restraint.

a, Simulation snapshot illustrating the geometry of the system. Shown is the central plane of the membrane (the lipid tail ends), the stalk, and HOPS. The SNARE complex present in the simulation setup is not illustrated. This setup serves as a motivation for the elastic continuum model. **b**, Bending work required to place HOPS at the (hemi-)fusion site and peristaltic force experienced by HOPS. Simulations were run to measure the work required to place HOPS-like spheres of 10–14 nm diameter at the site of hemifusion or at a fusion pore (FP). HOPS could be detached from the SNARE complex by a long spacer (link.). The influence of a SNARE complex with an unstructured, non-helical juxta-membrane region (unstr.) and of a HOPS mimic that was attractive to the membrane surface (attr.) was also analysed. The bottom panel shows averages obtained from the simulations. f_d is the (peristaltic) force that pushes HOPS away from the inter-membrane restraint (for example, a stalk, fusion pore, or *trans*-SNARE complex). Note that surface attractions or Rab-GTPase interactions of HOPS (modelling the tethering of membranes)^{10,47} can yield a negative value of the average work required to bend the membrane (bending occurs spontaneously). Fusion pore formation reduces the required bending work—it moves HOPS away from the restraint because of additional SNARE association up into the TMD region. The errors in the averages are derived from block averaging over more than 10,000 data points until the error becomes independent of block size (autocorrelation up to approximately 300 data points). **c**, Elastic

continuum model. The coordinate system is based on the snapshot of the molecular dynamics simulation shown in **a**. Because of symmetry along the x - y plane and x - z plane, we only model one-quarter of the original system. The cartoon illustrates the shape of minimal free energy for a membrane (modelled by a single sheet), subjected to two constraints: (1) A local constraint on the position (height) of the membrane illustrated by the black arrow at $z = 2$ nm. This mimics the inter-membrane constraint (stalk, fusion pore or partly-assembled SNARE complex). (2) The presence of a hemisphere, this mimics HOPS. The colour code illustrates the height of the membrane (the z axis) relative to the two constraints. **d**, Prediction of bending energies by the elastic continuum model. The bending energy is shown as a function of the size and distance of HOPS to the inter-membrane restraint. Top, bending energy decreases steeply when HOPS moves away from the restraint. The predicted values are about a factor of two lower than the ‘bending work’ predicted by the simulations (see Methods). Middle, the corresponding peristaltic force (f_d) on HOPS (the derivative of bending energy). At short distances, f_d becomes substantial (tens of pN). Note that making the surface of HOPS moderately attractive to the membrane affects f_d only weakly, that is, it does not result in an attraction towards the stalk. Bottom, the relative reduction of membrane area as a result of HOPS-induced membrane bending. This property reflects the tension that HOPS induces by curving the membrane near the contact zone. In contrast to bending energy and force, tension only weakly depends on the distance (d) to the restraint.



Extended Data Figure 10 | See next page for caption.

Extended Data Figure 10 | Effect of HOPS on the force exerted by a single SNARE complex. **a**, One way of rationalizing the acceleration of fusion pore formation by a SNARE complex is to consider it as a mechanical device that exerts force on the luminal leaflets through its TMDs, thereby compressing the stalk. This can happen through a peristaltic force that pulls the SNARE complex away from the stalk, or through the elastic bending of the SNAREs. This latter mode of force transmission requires the juxta-membrane regions, which connect the coiled-coil domains of the SNAREs to their TMDs, to be structured and rigid. The compressing force that the SNARE complex exerts on the stalk can be rationalized from the apparent work (free energy) that one needs to perform in order to force the luminal C termini of Vam3 and Nyv1 in closer proximity. We estimated how HOPS binding affects the force that the C termini of the SNAREs Vam3 and Nyv1 exert on the stalk. **b**, The work required to slightly indent the stalk in the presence of repulsive or attractive HOPS-spheres of different diameter has been determined. It is shown relative to the situation without the sphere. Error bars are calculated via Bayesian resampling of 15 overlapping WHAM histograms⁴². Each parental WHAM histogram is comprised of more than 30,000 data points (autocorrelation up to approximately 1,200 data points). The lines shown result from fitting a power expansion (up to the fourth power) through the average of each data point. Error bars are calculated via Bayesian resampling of 15 overlapping WHAM histograms⁴⁴. **c**, The corresponding forces on the SNARE TMDs were derived from this work. Apparent gains

in the force exerted by the SNARE C termini (left) are shown as a function of their distance in the hemifusion structure. HOPS binding can double or triple the magnitude of the apparent force (10–20 pN) that a SNARE complex exerts on a stalk⁵⁰. The gain dissipates, however, as zipping of the SNARE TMDs progresses and their C termini approach each other. **d**, Snapshots of three special scenarios. Top, The HOPS sphere is placed at a distal location with respect to the stalk (for example, via attachment with a flexible linker), which abolishes the force gain. Middle, A sphere that favourably attracts (and bends) the membrane, this conserves the force gain. Bottom, unstructured, flexible SNARE juxta-membrane regions partially disrupt the mechanical coupling between the coiled-coil domains and the TMDs; they decrease the apparent gain in SNARE pull force induced by HOPS. Structured (α -helical) SNARE juxta-membrane regions result in a high initial force gain which gradually reduces. In contrast, unstructured, flexible juxta-membrane regions, which impair vacuole fusion⁵¹, result in a near-constant force gain of only about 8 pN. Both cases converge to similar force values when the C termini of Vam3 and Nyv1 come in closer proximity. Because the SNARE complex is unable to exert bending force on the membrane, when the connection between its transmembrane anchors and the SNARE domains is completely flexible, we relate the remaining gain to an effective softening of the stalk because of the induced membrane curvature and to the peristaltic force generated by the interaction of the HOPS sphere with the SNAREs.

Life Sciences Reporting Summary

Nature Research wishes to improve the reproducibility of the work that we publish. This form is intended for publication with all accepted life science papers and provides structure for consistency and transparency in reporting. Every life science submission will use this form; some list items might not apply to an individual manuscript, but all fields must be completed for clarity.

For further information on the points included in this form, see [Reporting Life Sciences Research](#). For further information on Nature Research policies, including our [data availability policy](#), see [Authors & Referees](#) and the [Editorial Policy Checklist](#).

► Experimental design

1. Sample size

Describe how sample size was determined.

Sample sizes were chosen such that differences were confirmed at sufficiently high significance ($p < 0.005$) by Student's t-test

2. Data exclusions

Describe any data exclusions.

No data was excluded

3. Replication

Describe whether the experimental findings were reliably reproduced.

Experiments were repeated at least three times under identical conditions. These repetitions represent independent biological replicates.

4. Randomization

Describe how samples/organisms/participants were allocated into experimental groups.

Randomization was not performed

5. Blinding

Describe whether the investigators were blinded to group allocation during data collection and/or analysis.

Blinding techniques were not used.

Note: all studies involving animals and/or human research participants must disclose whether blinding and randomization were used.

6. Statistical parameters

For all figures and tables that use statistical methods, confirm that the following items are present in relevant figure legends (or in the Methods section if additional space is needed).

- | n/a | Confirmed |
|--------------------------|--|
| <input type="checkbox"/> | <input checked="" type="checkbox"/> The <u>exact sample size</u> (n) for each experimental group/condition, given as a discrete number and unit of measurement (animals, litters, cultures, etc.) |
| <input type="checkbox"/> | <input checked="" type="checkbox"/> A description of how samples were collected, noting whether measurements were taken from distinct samples or whether the same sample was measured repeatedly |
| <input type="checkbox"/> | <input checked="" type="checkbox"/> A statement indicating how many times each experiment was replicated |
| <input type="checkbox"/> | <input checked="" type="checkbox"/> The statistical test(s) used and whether they are one- or two-sided (note: only common tests should be described solely by name; more complex techniques should be described in the Methods section) |
| <input type="checkbox"/> | <input checked="" type="checkbox"/> A description of any assumptions or corrections, such as an adjustment for multiple comparisons |
| <input type="checkbox"/> | <input checked="" type="checkbox"/> The test results (e.g. P values) given as exact values whenever possible and with confidence intervals noted |
| <input type="checkbox"/> | <input checked="" type="checkbox"/> A clear description of statistics including <u>central tendency</u> (e.g. median, mean) and <u>variation</u> (e.g. standard deviation, interquartile range) |
| <input type="checkbox"/> | <input checked="" type="checkbox"/> Clearly defined error bars |

See the web collection on [statistics for biologists](#) for further resources and guidance.

► Software

Policy information about [availability of computer code](#)

7. Software

Describe the software used to analyze the data in this study.

The molecular dynamics simulations were performed with a self-modified version of the open source software Gromacs-4.5.5. The code is made publicly available under a link provided in Methods. Adobe Illustrator was used to assemble the figures. The software running the infrared laser scanner (LICOR Image Studio) was used to quantify the blots.

For manuscripts utilizing custom algorithms or software that are central to the paper but not yet described in the published literature, software must be made available to editors and reviewers upon request. We strongly encourage code deposition in a community repository (e.g. GitHub). *Nature Methods* [guidance for providing algorithms and software for publication](#) provides further information on this topic.

► Materials and reagents

Policy information about [availability of materials](#)

8. Materials availability

Indicate whether there are restrictions on availability of unique materials or if these materials are only available for distribution by a for-profit company.

None

9. Antibodies

Describe the antibodies used and how they were validated for use in the system under study (i.e. assay and species).

Antibodies were mouse monoclonals (HA, myc) or polyclonal antibodies raised in rabbits (Ypt7, Vps39, Vam3, Nyv1). Specificity of all antibodies was confirmed by Western blotting of material from respective knockout strains lacking the target protein, from strains lacking the peptide tag to which the antibody was directed. In the case of blots of co-IPs, specificity was verified by using conditions under which the interaction studied did not occur (Figs. 1a, 2d).

10. Eukaryotic cell lines

a. State the source of each eukaryotic cell line used.

n/a

b. Describe the method of cell line authentication used.

n/a

c. Report whether the cell lines were tested for mycoplasma contamination.

n/a

d. If any of the cell lines used are listed in the database of commonly misidentified cell lines maintained by [ICLAC](#), provide a scientific rationale for their use.

n/a

► Animals and human research participants

Policy information about [studies involving animals](#); when reporting animal research, follow the [ARRIVE guidelines](#)

11. Description of research animals

Provide details on animals and/or animal-derived materials used in the study.

n/a

Policy information about [studies involving human research participants](#)

12. Description of human research participants

Describe the covariate-relevant population characteristics of the human research participants.

n/a